
REASONABLE MECHANICAL MODEL ON SHALLOW TUNNEL EXCAVATION TO ELIMINATE DISPLACEMENT SINGULARITY CAUSED BY UNBALANCED RESULTANT

A PREPRINT

 **Luobin Lin**

Fujian Provincial Key Laboratory of Advanced Technology and Informatization in Civil Engineering

College of Civil Engineering

Fujian University of Technology

No. 69 Xueyuan Road, Shangjie University Town, Fuzhou, 350118, Fujian, China

luobin.lin@fjut.edu.cn

 **Fuquan Chen**

College of Civil Engineering

Fuzhou University

No. 2 Xueyuan Road, Shangjie University Town, Fuzhou, 350108, Fujian, China

phdchen@fzu.edu.cn

 **Xianhai Huang**

College of Civil Engineering

Fujian University of Technology

No. 69 Xueyuan Road, Shangjie University Town, Fuzhou, 350118, Fujian, China

hwhsh@163.com

August 9, 2023

ABSTRACT

When considering initial stress field in geomaterial, nonzero resultant of shallow tunnel excavation exists, which produces logarithmic items in complex potentials, and would further lead to a unique displacement singularity at infinity to violate geo-engineering fact in real world. The mechanical and mathematical reasons of such a unique displacement singularity in the existing mechanical models are elaborated, and a new mechanical model is subsequently proposed to eliminate this singularity by constraining far-field ground surface displacement, and the original unbalanced resultant problem is converted into an equilibrium one with mixed boundary conditions. To solve stress and displacement in the new model, the analytic continuation is applied to transform the mixed boundary conditions into a homogenous Riemann-Hilbert problem with extra constraints, which is then solved using

an approximate and iterative method with good numerical stability. The Lanczos filtering is applied to the stress and displacement solution to reduce the Gibbs phenomena caused by abrupt change of the boundary conditions along ground surface. Several numerical cases are conducted to verify the proposed mechanical model and the results strongly validate that the proposed mechanical model successfully eliminates the displacement singularity caused by unbalanced resultant with good convergence and accuracy to obtain stress and displacement for shallow tunnel excavation. A parametric investigation is subsequently conducted to study the influence of tunnel depth, lateral coefficient, and free surface range on stress and displacement distribution in geomaterial.

Keywords Shallow tunnel excavation · Unbalanced resultant · Displacement singularity · Analytic continuation · Riemann-Hilbert problem

1 Introduction

Shallow tunnel excavation is common in geo-engineering. Owing to initial stress field, the stress difference between top and bottom of a shallow tunnel always exists prior to excavation, and a subsequent excavation would alter stress and displacement distribution of geomaterial in a more mechanically complicated way than a deep tunnel. Moreover, the gravity of the excavated geomaterial can not be neglected comparing to the initial stress field, and the gravity gradient in geomaterial would also cause unbalanced resultant along tunnel periphery.

An unbalanced resultant is mathematically challenging in the complex variable method, since it brings a logarithmic item in the complex potentials. Muskhelishvili [1966] has pointed out that the logarithmic item in complex potential may result in displacement singularity. Strack [2002] introduces an extra singularity in the upper half plane and the other corresponding logarithmic item into Muskhelishvili's complex potentials to meet the stress equilibrium in the lower half plane, but the displacement singularity at infinity caused by the unbalanced resultant along tunnel periphery still exists. With the modified complex potentials by Strack [Strack, 2002] and Verruijt's conformal mapping [Verruijt, 1997b,a], Verruijt and Strack [Strack and Verruijt, 2002] and Lu et al. [Lu et al., 2016] propose solutions of different boundary conditions along tunnel periphery with unbalanced resultant of shallow tunnel excavation. Lu et al. [Lu et al., 2019] introduces the analytic continuation for free traction boundary along the whole ground surface to simplify the solution procedure and studies the stress and displacement in geomaterial for a shallow tunnel excavation subjected to underground water. Fang et al. [Fang et al., 2015] studies the stress and displacement of a underwater shallow tunnel excavation. Zeng et al. [Zeng et al., 2019] proposes a new conformal mapping for a noncircular cavity in a lower half plane, which is an extension of Verruijt's conformal mapping, and studies the stress and displacement in geomaterial due a noncircular shallow tunnel excavation. However, the displacement singularity at infinity is still not eliminated. The static equilibrium problems of shallow tunnel are also studied [Zhang et al., 2018, Kong et al., 2019, 2021]. The displacement singularity is not only observed in complex variable method, but also in the stress function method of real domain Timoshenko and Goodier [1951], where a similar logarithmic item also exists in the stress potential.

Unbalanced resultant may also be induced by surcharge loads along ground surface. The classic Flamant solution [Flamant, 1892] has shown that an unbalanced resultant on ground surface would cause displacement singularity

at infinity as well. Wang et al. [Wang et al., 2017] propose a reasonable displacement model based on the Flamant's solution via symmetrical modification, and good results are obtained. Wang et al. [Gao et al., 2021, Wang et al., 2018b,a] then propose further studies on surcharge loads acting on ground surface of shallow tunnel, but no excavation process is considered, based on the symmetrical modification [Wang et al., 2017]. Zeng et al. [Zeng et al., 2022] also studies the visco-elastic mechanical behaviour of noncircular shallow tunnel on the symmetrical modification [Wang et al., 2017]. Zhang et al. [Zhang et al., 2021] study the visco-elastic deformation in visco-elastic geomaterial when surcharge loads is subjected on the ground surface. Inspired by Ref [Wang et al., 2017], Lin et al. [Lin et al., 2020] propose an extended displacement model of symmetrical modification for both surcharge load on ground surface and unbalanced resultant along shallow tunnel periphery for excavation, which indeed eliminates the displacement singularity, but displacement solution is highly dependent on the modification depth. In other words, the convergence of displacement is not as good as expected. Lu et al. [Lu et al., 2021] modify the the coefficients of the Taylor expansion of the logarithmic item to obtain reasonable displacement distribution when a surcharge load of Gaussian distribution is applied on the ground surface. However, the solution [Lu et al., 2021] is dependent on the constant in conformal mapping, which is corresponding to the complex coordinate of the mapping point in the physical plane of the unit disk origin. The value of this constant can be arbitrarily chosen, since a lower half plane without any cavity is simply connected. The solution by Lu et al. [Lu et al., 2021] is unsurprisingly not suitable for unbalanced resultant problem of shallow tunnel excavation, since that constant should be unique for the remaining geomaterial after shallow tunnel excavation [Verruijt, 1997b,a], which is a doubly connected region.

In summary, the displacement singularity caused by the logarithmic item in complex potentials is still not eliminated in the existing studies of shallow tunnel excavation, or the elimination is not as good as expected. For such reasons, we propose a new model in this study to confront the displacement singularity caused by unbalanced resultant of shallow tunnel excavation in a very straightforward and mechanical manner by introducing the analytic continuation and Riemann-Hilbert problem of mixed boundary value conditions into theoretical analyses in tunnel engineering.

2 Problem formation

2.1 Existing mechanical model of shallow tunnel excavation

We start with a common model for shallow tunnelling in a heavy geomaterial in a lower half plane, similar to the cases in Refs Strack [2002], Strack and Verruijt [2002], Lu et al. [2016], Zeng et al. [2019], Lin et al. [2020]. As shown in Fig. 1a, a geomaterial Ω located in a complex lower half plane $z(z = x + iy)$ is linearly elastic, homogenous, isotropic, of small deformation, and is subjected to a uniform intial stress field, which can be expressed as

$$\begin{cases} \sigma_x^0 = k_0 \gamma y \\ \sigma_y^0 = \gamma y \quad , \quad y \leq 0 \\ \tau_{xy}^0 = 0 \end{cases} \quad (2.1)$$

where σ_x^0 , σ_y^0 , and τ_{xy}^0 denote horizontal, vertical, and shear stress components of the initial stress field in the rectangular coordinate system xOy , k_0 denotes lateral stress coefficient, γ denotes volumetric weight of geomaterial. The ground surface denoted by C_1 is fully free from any traction.

Then a shallow tunnel with radius of R and buried depth of h is excavated in the geomaterial of the lower half plane, and the tunnel periphery is denoted by C_2 . The following external tractions are applied to tunnel periphery to cancel the tractions caused by the initial stress field as shown in Fig. 1b:

$$\begin{cases} X_i(S) = -\sigma_x^0(S) \cdot \cos\langle\vec{n}, x\rangle - \tau_{xy}^0(S) \cdot \cos\langle\vec{n}, y\rangle \\ Y_i(S) = -\sigma_y^0(S) \cdot \cos\langle\vec{n}, y\rangle - \tau_{xy}^0(S) \cdot \cos\langle\vec{n}, x\rangle \end{cases}, \quad S : x^2 + (y + h)^2 = R^2 \quad (2.2)$$

where $X_i(S)$ and $Y_i(S)$ denote horizontal and vertical traction along tunnel periphery C_2 (denoted by S), respectively, \vec{n} denotes the outward direction along the tunnel periphery, as shown in Fig. 1b, $\langle\vec{n}, x\rangle$ denotes angle between \vec{n} and x axis, and $\langle\vec{n}, y\rangle$ denotes angle between \vec{n} and y axis. The initial stress field in Eq. (2.1) and the tractions in Eq. (2.2) together keep the tunnel periphery being traction-free. A local polar coordinate system $\varrho\vartheta$ is introduced and located at the center of the tunnel, and Eq. (2.2) turns to

$$\begin{cases} X_i(S) = X_i(\vartheta) = k_0\gamma(-h + R\sin\vartheta)\cos\vartheta \\ Y_i(S) = Y_i(\vartheta) = \gamma(-h + R\sin\vartheta)\sin\vartheta \end{cases} \quad (2.3)$$

Integrating the tractions along tunnel periphery in the clockwise direction (keeping the geomaterial on the left side) gives the following unbalanced resultants along tunnel periphery C_2 :

$$\begin{cases} F_x = \oint_{C_2} X_i(S)|dS| = -\oint_{C_2} X_i(\vartheta)Rd\vartheta = 0 \\ F_y = \oint_{C_2} Y_i(S)|dS| = -\oint_{C_2} Y_i(\vartheta)Rd\vartheta = \gamma\pi R^2 \end{cases} \quad (2.4)$$

where F_x and F_y denote horizontal and vertical components of the resultant acting along boundary C_2 , respectively; $|dS| = R|d\vartheta| = -Rd\vartheta$ for clockwise length increment in physical plane. To be more specific, the value of the total gravity of the excavated geomaterial should be $-\gamma\pi R^2$, and the positive value of F_y indicates the removal action of the excavated geomaterial and the corresponding external force applied to the tunnel periphery C_2 .

2.2 Unbalanced resultant and displacement singularity of existing mechanical model

With the unbalanced resultant in Eq. (2.4), the excavation process is illustrated in Fig. 2a, where the unbalanced resultant denoted by \vec{F}_1 ($|\vec{F}_1| = F_y$) is equivalently applied at singularity S_1 within tunnel. Though such equivalence is not accurate enough, it helps to simplify our description below in a rough sense. Then the complex potentials $\varphi(z)$ and $\psi(z)$ related to the unbalanced resultant can be constructed according to Eqs. (4.1) and (4.2) in Ref Strack [2002], Eqs. (7) and (8) in Ref Strack and Verruit [2002], Eqs. (17) and (18) in Ref Lu et al. [2016], or Eq. (24) in Ref Lin et al. [2020] as

$$\varphi(z) = -\frac{F_x + iF_y}{2\pi(1+\kappa)} [\kappa \ln(z - \bar{z}_c) + \ln(z - z_c)] + \varphi_0(z), \quad z \in \Omega \quad (2.5a)$$

$$\psi(z) = \frac{F_x - iF_y}{2\pi(1+\kappa)} [\ln(z - \bar{z}_c) + \kappa \ln(z - z_c)] + \psi_0(z), \quad z \in \Omega \quad (2.5b)$$

where z_c denotes the complex coordinate of point S_1 within the tunnel, \bar{z}_c denotes the complex coordinate of the corresponding conjugate point S_2 in the upper half plane, $\varphi_0(z)$ and $\psi_0(z)$ denote the single-valued components of the complex potentials, which are always finite in the geomaterial.

With Eq. (2.4), Eq. (2.5) can be simplified and rewritten as

$$\varphi(z) = \left[-\frac{iF_y}{2\pi} \ln(z - \bar{z}_c) - \frac{-iF_y}{2\pi(1+\kappa)} \ln(z - z_c) \right] - \frac{iF_y}{2\pi(1+\kappa)} \ln(z - z_c) + \varphi_0(z), \quad z \in \Omega \quad (2.6a)$$

$$\psi(z) = \left[-\frac{iF_y}{2\pi} \ln(z - \bar{z}_c) + \frac{i\kappa F_y}{2\pi(1 + \kappa)} \ln(z - \bar{z}_c) \right] + \frac{-i\kappa F_y}{2\pi(1 + \kappa)} \ln(z - z_c) + \psi_0(z), \quad z \in \Omega \quad (2.6b)$$

where the first two logarithmic items take point S_2 in the upper-half plane as singularity, and the last logarithmic item takes point S_1 in the lower-half plane as singularity. Since the geomaterial has been assumed to be of small deformation, we can respectively examine the logarithmic items in Eq. (2.6). Apparently, the second and third logarithmic items in Eq. (2.6) indicate that an upward and a downward concentrated resultant acting at singularities S_2 and S_1 , respectively, according to § 56a in Ref [Muskhelishvili, 1966], and the downward concentrated resultant is denoted by $\vec{F}_2 (|\vec{F}_2| = F_y)$ in Fig. 2c. Meanwhile, the first logarithmic item in Eq. (2.6) indicates an upward concentrated resultant acting at *some point on the boundary* of the singularity S_2 *after the existence of the singularity in the upper-half plane*, according to § 90 in Ref [Muskhelishvili, 1966], and such an upward resultant is denoted by $\vec{F}_3 (|\vec{F}_3| = F_y)$ in Fig. 2c.

Since the singularity S_2 is just a point, its boundary is itself. To guarantee the existence of its boundary, the only possible solution is that the upper-half plane should be fully defined except for the singularity S_2 , otherwise, the expression of the first logarithmic item in Eq. (2.6) would be violated. In other words, the expression form of Eq. (2.6) implicitly indicates that the analytic continuation principle has been applied *across the full length of the ground surface*. Since the ground surface is always traction free, the analytic continuation principle is reduced to be the traction continuation [Muskhelishvili, 1966], as shown in Fig. 2c. In Fig. 2c, \vec{F}_2 and \vec{F}_3 are a pair of equilibrium resultants. The application of the analytic continuation principle does not conflict with the deduction process of obtaining Eq. (2.5) in Ref [Strack, 2002], and the geomaterial remains a doubly connected region before and after application of the analytic continuation principle in Fig. 2c.

According associative law of addition, Eq. (2.6) can be further modified as

$$\varphi(z) = -\frac{iF_y}{2\pi} \ln(z - \bar{z}_c) + \frac{-iF_y}{2\pi(1 + \kappa)} \ln \frac{z - z_c}{z - \bar{z}_c} + \varphi_0(z), \quad z \in \Omega \quad (2.7a)$$

$$\psi(z) = -\frac{iF_y}{2\pi} \ln(z - \bar{z}_c) + \frac{-i\kappa F_y}{2\pi(1 + \kappa)} \ln \frac{z - z_c}{z - \bar{z}_c} + \psi_0(z), \quad z \in \Omega \quad (2.7b)$$

Eq. (2.7) indicates that \vec{F}_1 and \vec{F}_2 are set to a new pair of equilibrium resultants, and \vec{F}_3 is left alone, as shown in 2d. No matter for the mechanical models in Fig. 2c or 2d, no static equilibrium can be established, which is hazardous to obtain fully reasonable stress and displacement. To verify such a hazard, we could examine the stress and displacement for the complex potentials in Eq. (2.7).

The stress and displacement components within geomaterial in the physical plane $z(xOy)$ can be given as

$$\begin{cases} \sigma_y(z) + \sigma_x(z) = 2 \left[\frac{d\varphi(z)}{dz} + \overline{\frac{d\varphi(z)}{dz}} \right] \\ \sigma_y(z) - \sigma_x(z) + 2i\tau_{xy}(z) = 2 \left[\bar{z} \frac{d^2\varphi(z)}{dz^2} + \frac{d\psi(z)}{dz} \right], \end{cases} \quad z \in \Omega \quad (2.8a)$$

$$g(z) = 2G [u(z) + iv(z)] = \kappa\varphi(z) - z \frac{\overline{d\varphi(z)}}{dz} - \overline{\psi(z)}, \quad z \in \Omega \quad (2.8b)$$

where $\sigma_x(z)$, $\sigma_y(z)$, and $\tau_{xy}(z)$ denote horizontal, vertical, and shear stress components, respectively; $u(z)$ and $v(z)$ denote horizontal and vertical displacement components, respectively; $G = \frac{E}{2(1+\nu)}$ denotes shear modulus of geomaterial, E and ν denote elastic modulus and poisson's ratio of geomaterial, respectively, κ denotes the Kolosov coefficient with $\kappa = 3 - 4\nu$ for plane strain and $\kappa = \frac{3-\nu}{1+\nu}$ for plane stress, and ν denotes the Poisson's ratio of geomaterial.

When substituting Eq. (2.7) into Eq. (2.8), we can find that the stress components are always finite, whereas the displacement components would be infinite when z approach infinity, indicating a unique displacement singularity at infinity. Such a property has been reported in Ref Lin et al. [2020], where a symmetrical modification is provided to attempt to fix the unique displacement singularity. However, the modification strategy in Ref Lin et al. [2020] still depends on the modification depth (an exogenous parameter), and consequently the convergence is not as good as expected, which is shown in the numerical cases in Section 6.3.

Therefore, we should seek a more reasonable strategy to equilibrate the unbalanced resultant \vec{F}_1 and to constrain the unique displacement singularity at infinity. To simultaneously achieve both goals, we propose a new mechanical model in Fig. 2b, where displacement along the far-field ground surface is symmetrically constrained. Apparently, the displacement constraint along far-field ground surface would provide a constraining force to equilibrate the unbalanced resultant \vec{F}_1 acting at singularity S_1 , thus, the originally unbalanced problem in Refs Strack [2002], Strack and Verruijt [2002], Lu et al. [2016], Zeng et al. [2019], Lin et al. [2020] would turn to a balanced one. Furthermore, the displacement constraint along far-field ground surface can be expected to literally and mechanically constrain the displacement singularity at infinity. The ground surface turns from a fully free one to a partially free one, as shown in Fig. 2b.

2.3 Mixed boundary value problem and conformal mapping

The mechanical model in Fig. 2b is no longer similar to the above mentioned ones in Refs Strack [2002], Strack and Verruijt [2002], Lu et al. [2016], Zeng et al. [2019], Lin et al. [2020], but is a mixed boundary value problem of elasticity. The ground surface is separated into the displacement-constrained segment C_{11} and the partially free segment C_{12} , as shown in Fig. 3a. Both segments are axisymmetrical, and the intersection points between C_{11} and C_{12} are denoted by T_1 and T_2 , respectively. The following mixed boundary conditions can be constructed according to the mechanical model in Fig. 3a: far-field ground surface (C_{11}) is constrained, and the rest part (C_{12}) is free, and the tunnel periphery (C_2) is subjected to tractions in Eq. (2.3) with resultants in Eq. (2.4). Apparently, the constrained far-field ground surface would produce a constraining force to equilibrate the unbalanced resultant along shallow tunnel periphery. In other words, the unbalanced model proposed by Strack [Strack, 2002] is modified to the static equilibrium model with mixed boundary conditions in this paper.

The boundary conditions along the ground surface can be expressed in the complex variable manner as

$$u(T) + iv(T) = 0, \quad T \in C_{11} \quad (2.9a)$$

$$X_o(T) + iY_o(T) = 0, \quad T \in C_{12} \quad (2.9b)$$

where $u(T)$ and $v(T)$ denote the horizontal and vertical displacement components along boundary C_{11} , respectively; $X_o(T)$ and $Y_o(T)$ denote horizontal and vertical tractions along boundary C_{12} , respectively. Apparently, Eq. (2.9) already contains mixed boundary conditions.

Considering the mathematical equilibriums $\cos\langle\vec{n}, x\rangle = \frac{dy}{dS}$ and $\cos\langle\vec{n}, y\rangle = -\frac{dx}{dS}$ owing to outward normal vector \vec{n} and clockwise positive direction of tunnel periphery, Eq. (2.2) can be rewritten as

$$\begin{cases} X_i(S) = -k_0\gamma y \frac{dy}{dS}, \\ Y_i(S) = \gamma y \frac{dx}{dS} \end{cases}, \quad S : x^2 + (y + h)^2 = R^2 \quad (2.2')$$

Eq. (2.2') is the boundary condition along tunnel periphery, and is similar to those boundary conditions in the previously mentioned studies Lu et al. [2016], Zeng et al. [2019], Lin et al. [2020]. Eqs. (2.9) and (2.2') form the necessary mathematical expressions for the mixed boundary value problem.

For better use of Eqs. (2.9) and (2.2'), the Verruijt's conformal mapping [Verruijt, 1997b,a] is applied to map the geomaterial with a shallow circular tunnel in a lower half plane onto the unit annulus with inner radius of r (denoted by ω in Fig. 3b) in a bidirectional manner via the following mapping functions:

$$\zeta(z) = \frac{z + ia}{z - ia} \quad (2.10a)$$

$$z(\zeta) = -ia \frac{1 + \zeta}{1 - \zeta} \quad (2.10b)$$

where

$$\begin{cases} a = h \frac{1 - r^2}{1 + r^2} \\ r = \frac{R}{h + \sqrt{h^2 - R^2}} \end{cases} \quad (2.11)$$

Via the conformal mapping functions in Eq. (2.10), the boundaries C_{11} , C_{12} , and C_2 in the lower half plane in Fig. 3a are respectively mapped onto c_{11} , c_{12} , and c_2 in the unit annulus in Fig. 3b in a bidirectional manner. Boundaries c_{11} and c_{12} together can be denoted by c_1 . Corresponding to region Ω in the physical plane z , region ω in the mapping plane ζ is also a closure that contains c_1 , c_2 , and the unit annulus bounded by both boundaries. It should be addressed that since the infinity point $z = \infty$ in the lower half plane is mapped onto point $\zeta = 1$ in the unit annulus, the infinite boundary C_{11} is mapped onto a finite arc c_{11} correspondingly. The intersection points T_1 and T_2 are also mapped onto points t_1 and t_2 , respectively. Since T_1 and T_2 are axisymmetrical, t_1 and t_2 would also be axisymmetrical. Assume that the horizontal coordinates of points T_1 and T_2 are $-x_0$ and x_0 , respectively; then the polar angles of points t_1 and t_2 would be $-\theta_0$ and θ_0 , respectively, where $\theta_0 = -i \ln \frac{x_0 + ia}{x_0 - ia}$.

The mixed boundary conditions in the lower half plane in Eq. (2.9) and (2.2') can also be conformally mapped onto the ones in the unit annulus as

$$u(t) + iv(t) = u(T) + iv(T) = 0, \quad t = e^{i\theta} \in c_{11} \quad (2.12a)$$

$$e^{i\theta} \frac{z'(t)}{|z'(t)|} \cdot [\sigma_\rho(t) + i\tau_{\rho\theta}(t)] = X_o(T) + iY_o(T) = 0, \quad t = e^{i\theta} \in c_{12} \quad (2.12b)$$

$$e^{i\theta} \frac{z'(s)}{|z'(s)|} \cdot [\sigma_\rho(s) + i\tau_{\rho\theta}(s)] = X_i(S) + iY_i(S) = -k_0 \gamma y \frac{dy}{dS} + i\gamma y \frac{dx}{dS}, \quad s = re^{i\theta} \in c_2 \quad (2.12c)$$

where the points t and s in the unit annulus are respectively corresponding to the points T and S in the lower half plane; σ_ρ and $\tau_{\rho\theta}$ denote radial and shear stress components, respectively; $z'(t)$ and $z'(s)$ denote taking derivatives of $z(t)$ and $z(s)$, respectively. Now we should solve the mixed boundary value problem in Eq. (2.12).

3 Analytic continuation and Riemann-Hilbert problem

To solve the mixed boundary value problem in Eq. (2.12) and to obtain stress and displacement solution of shallow tunnel excavation, the analytic continuation [Muskhelishvili, 1966] is applied to the proposed mechanical model. Considering the backward conformal mapping in Eq. (2.10b), the stress and displacement in geomaterial in Eq. (2.8) can be mapped onto the mapping plane ζ as

$$\sigma_\theta(\zeta) + \sigma_\rho(\zeta) = 2 [\Phi(\zeta) + \overline{\Phi(\zeta)}], \quad \zeta \in \omega \quad (3.1a)$$

$$\sigma_\rho(\zeta) + i\tau_{\rho\theta}(\zeta) = \Phi(\zeta) + \overline{\Phi(\zeta)} - e^{-2i\theta} \left[\frac{z(\zeta)}{z'(\zeta)} \overline{\Phi'(\zeta)} + \frac{\overline{z'(\zeta)}}{z'(\zeta)} \overline{\Psi(\zeta)} \right], \quad \zeta \in \omega \quad (3.1b)$$

$$g(\zeta) = 2G [u(\zeta) + iv(\zeta)] = \kappa\varphi(\zeta) - z(\zeta)\overline{\Phi(\zeta)} - \overline{\psi(\zeta)}, \quad \zeta \in \omega \quad (3.1c)$$

where

$$\begin{cases} \Phi(\zeta) = \frac{\varphi'(\zeta)}{z'(\zeta)} \\ \Psi(\zeta) = \frac{\psi'(\zeta)}{z'(\zeta)} \end{cases}$$

Eq. (3.1a) requires $\Phi(\zeta)$ to be analytic within region ω , and Eq. (3.1b) further requires the last two items on the right-hand side to be analytic within region ω , which can be expanded as

$$\begin{cases} \frac{z(\zeta)}{z'(\zeta)} \overline{\Phi'(\zeta)} = \frac{1 - \zeta^2}{2} \overline{\Phi'(\zeta)} \\ \frac{z'(\zeta)}{z'(\zeta)} \overline{\Psi(\zeta)} = -(1 - \zeta)^2 \frac{\overline{\Psi(\zeta)}}{(1 - \bar{\zeta})^2} \end{cases}, \quad \zeta \in \omega \quad (3.2a)$$

The first equation in Eq. (3.2a) is apparently analytic within region ω , and the second equation would be analytic within region ω , as long as $\Psi(\zeta)$ can be expressed as multiplication of $(1 - \zeta)$ and an analytic function without any singularity in region ω , because

$$\lim_{\zeta \rightarrow 1} \frac{(1 - \zeta)^2}{1 - \bar{\zeta}} = \lim_{\zeta \rightarrow 0} \frac{\zeta^2}{\bar{\zeta}} = \lim_{\rho \rightarrow 0} \frac{\rho^2}{\rho} e^{3i\theta} = 0$$

always stands. Eq. (3.2a) indicates that $\zeta = 1$ should not be a singularity point for stress.

The complex potentials in Eq. (3.1c) can be expanded as

$$\begin{cases} \varphi(\zeta) = \int \varphi'(\zeta) d\zeta = \int z'(\zeta) \Phi(\zeta) d\zeta = -2ia \int \frac{\Phi(\zeta)}{(1 - \zeta)^2} d\zeta \\ \psi(\zeta) = \int \psi'(\zeta) d\zeta = \int z'(\zeta) \Psi(\zeta) d\zeta = -2ia \int \frac{\Psi(\zeta)}{(1 - \zeta)^2} d\zeta \end{cases}, \quad \zeta \in \omega \quad (3.2b)$$

Eq. (3.2b) indicates that $\zeta = 1$ may be a second-order singularity point. However, according to Eq. (2.12a), displacement along the whole boundary c_{11} should be equal to zero, including point $\zeta = 1$. Eq. (3.2b) should therefore be analytic within region ω , as long as $\Phi(\zeta)$ and $\Psi(\zeta)$ can be expressed as a multiplication of $(1 - \zeta)^2$ and an analytic function in region ω without any singularity. Eq. (3.2b) indicates that displacement has a stronger requirement on $\Phi(\zeta)$ and $\Psi(\zeta)$, comparing to stress in Eq. (3.2a). In other words, Eqs. (3.2a) and (3.2b) both require that the possible second-order singularity $\zeta = 1$ in $z'(\zeta)$ should not be a singularity point for $z'(\zeta)\Phi(\zeta)$ and $z'(\zeta)\Psi(\zeta)$, as well as $\Phi(\zeta)$ and $\Psi(\zeta)$. Eq. (3.1c) further requires the remaining item to be analytic within region ω , which can be expanded as

$$z(\zeta)\overline{\Phi(\zeta)} = \overline{z'(\zeta)\Phi(\zeta)} \cdot \frac{z(\zeta)}{z'(\zeta)} = -\frac{1 + \zeta}{2} \overline{z'(\zeta)\Phi(\zeta)} \cdot \frac{(1 - \bar{\zeta})^2}{1 - \zeta}, \quad \zeta \in \omega \quad (3.2c)$$

Whether or not Eq. (3.2c) is analytic within region ω depends on the last item on the possible singularity point $\zeta = 1$, which can be computed in a similar manner above:

$$\lim_{\zeta \rightarrow 1} \frac{(1 - \bar{\zeta})^2}{1 - \zeta} = \lim_{\zeta \rightarrow 0} \frac{\bar{\zeta}^2}{\zeta} = \lim_{\rho \rightarrow 0} \frac{\rho^2}{\rho} e^{-3i\theta} = 0$$

Eqs. (3.2b) and (3.2c) indicate that $\zeta = 1$ should not be a singularity point for displacement as well.

With the multiplier $(1 - \zeta)^2$ in $\Phi(\zeta)$ and $\Psi(\zeta)$, the stress components would vanish at point $\zeta = 1$ in the mapping plane according to Eqs. (3.1a) and (3.1b), correspondingly indicating that the stress components at infinity in the

physical plane would vanish. Such a result is identical to our expectation. Moreover, owing to the axisymmetry of the mechanical model, no far-field rotation or moment need be considered.

Therefore, before any further discussion, we find that $\Phi(\zeta)$ and $\Psi(\zeta)$, as well as $z'(\zeta)\Phi(\zeta)$ and $z'(\zeta)\Psi(\zeta)$, should be analytic within region ω without any singularity. To facilitate our discussion, we denote the regions $r \leq \rho < 1$ and $1 < \rho \leq r^{-1}$ by ω^+ and ω^- , respectively, as shown in Fig. 3b, and $\omega = \omega^+ \cup c_1$. Apparently, $\Phi(\zeta)$ and $\Psi(\zeta)$, as well as $z'(\zeta)\Phi(\zeta)$ and $z'(\zeta)\Psi(\zeta)$, are all analytic within region ω^+ . The analytic continuation principle will be used below to find solution of the stress and displacement components in the unit annulus in Eq. (3.1), according to the mixed boundary conditions in Eq. (2.12).

Substituting Eq. (3.1b) into Eq. (2.12b) and noting $\bar{t} = t^{-1}$ yields

$$\Phi(t) = -\bar{\Phi}(t^{-1}) + \frac{1}{t^2} \left[\frac{z(t)}{z'(t)} \bar{\Phi}'(t^{-1}) + \frac{\bar{z}'(t^{-1})}{z'(t)} \bar{\Psi}(t^{-1}) \right], \quad t = e^{i\theta} \in c_{12} \quad (3.3)$$

Replacing t with $\zeta = \rho \cdot e^{i\theta}$ ($1 < \rho \leq r^{-1}$), Eq. (3.3) would turn to

$$\Phi(\zeta) = -\bar{\Phi}(\zeta^{-1}) + \frac{1}{\zeta^2} \left[\frac{z(\zeta)}{z'(\zeta)} \bar{\Phi}'(\zeta^{-1}) + \frac{\bar{z}'(\zeta^{-1})}{z'(\zeta)} \bar{\Psi}(\zeta^{-1}) \right], \quad \zeta = \rho \cdot e^{i\theta} \in \omega^-(1 < \rho \leq r^{-1}) \quad (3.4)$$

The polar radius range $1 < \rho \leq r^{-1}$ ensure all the items of the right-hand side of Eq. (3.4) to be analytic. Eq. (3.4) can be modified as

$$z'(\zeta)\Phi(\zeta) = -z'(\zeta)\bar{\Phi}(\zeta^{-1}) + \frac{1}{\zeta^2} z(\zeta) \bar{\Phi}'(\zeta^{-1}) + \frac{1}{\zeta^2} \bar{z}'(\zeta^{-1}) \bar{\Psi}(\zeta^{-1}), \quad \zeta = \rho \cdot e^{i\theta} \in \omega^-(1 < \rho \leq r^{-1}) \quad (3.5)$$

Eq. (3.5) shows that $z'(\zeta)\Phi(\zeta)$ is analytic within region ω^- ($1 < \rho \leq r^{-1}$) without any singularity point. Combining with Eqs. (3.2), $z'(\zeta)\Phi(\zeta)$ should be analytic within the region $\omega^+ \cup c_1 \cup \omega^-$ without any singularity point. Replacing ζ with $\bar{\zeta}^{-1}$ in Eq. (3.5) and taking conjugate yields

$$z'(\zeta)\Psi(\zeta) = \frac{1}{\zeta^2} \bar{z}'(\zeta^{-1}) \bar{\Phi}(\zeta^{-1}) + \frac{1}{\zeta^2} \bar{z}'(\zeta^{-1}) \Phi(\zeta) - \bar{z}(\zeta^{-1}) \Phi'(\zeta), \quad \zeta = \rho \cdot e^{i\theta} \in \omega^+(r \leq \rho < 1) \quad (3.6)$$

Eq. (3.6) shows that $z'(\zeta)\Psi(\zeta)$ is defined and analytic within region ω^+ without any singularity point, and can be expressed by combination of $\Phi(\zeta)$ in regions ω^+ and ω^- . Thus, we only need to focus on $z'(\zeta)\Phi(\zeta)$.

Integrating Eq. (3.5) by ζ yields

$$\varphi(\zeta) = -z(\zeta)\bar{\Phi}(\zeta^{-1}) - \bar{\psi}(\zeta^{-1}) + \text{constant}, \quad \zeta = \rho \cdot e^{i\theta} \in \omega^-(1 < \rho \leq r^{-1}) \quad (3.7)$$

Replacing ζ with $\bar{\zeta}^{-1}$ in Eq. (3.8) yields

$$\varphi(\bar{\zeta}^{-1}) = -z(\bar{\zeta}^{-1}) \bar{\Phi}(\zeta) - \bar{\psi}(\zeta) + \text{constant}, \quad \zeta = \rho \cdot e^{i\theta} \in \omega^+(r \leq \rho < 1) \quad (3.8)$$

Taking derivative of $\bar{\zeta}$ in Eq. (3.8) yields

$$\Phi(\bar{\zeta}^{-1}) = \bar{\zeta}^2 \frac{z(\bar{\zeta}^{-1})}{z'(\bar{\zeta}^{-1})} \bar{\Phi}'(\zeta) + \bar{\zeta}^2 \frac{\bar{z}'(\zeta)}{z'(\bar{\zeta}^{-1})} \bar{\Psi}(\zeta) - \bar{\Phi}(\zeta), \quad \zeta = \rho \cdot e^{i\theta} \in \omega^+(r \leq \rho < 1) \quad (3.9)$$

Eq. (3.9) can be transformed as

$$\bar{\Phi}(\zeta) = -\Phi(\bar{\zeta}^{-1}) + \bar{\zeta}^2 \frac{z(\bar{\zeta}^{-1})}{z'(\bar{\zeta}^{-1})} \bar{\Phi}'(\zeta) + \bar{\zeta}^2 \frac{\bar{z}'(\zeta)}{z'(\bar{\zeta}^{-1})} \bar{\Psi}(\zeta), \quad \zeta = \rho \cdot e^{i\theta} \in \omega^+(r \leq \rho < 1) \quad (3.10)$$

Substituting Eq. (3.10) into Eq. (3.1b) yields

$$\begin{aligned} \sigma_\rho(\zeta) + i\tau_{\rho\theta}(\zeta) &= \bar{\zeta}^2 \left[\frac{z(\bar{\zeta}^{-1})}{z'(\bar{\zeta}^{-1})} - \frac{1}{\rho^2} \frac{z(\zeta)}{z'(\zeta)} \right] \bar{\Phi}'(\zeta) + \bar{\zeta}^2 \left[\frac{\bar{z}'(\zeta)}{z'(\bar{\zeta}^{-1})} - \frac{1}{\rho^2} \frac{\bar{z}'(\zeta)}{z'(\zeta)} \right] \bar{\Psi}(\zeta) \\ &\quad + \Phi(\zeta) - \Phi(\bar{\zeta}^{-1}), \quad \zeta = \rho \cdot e^{i\theta} \in \omega^+ (r \leq \rho < 1) \end{aligned} \quad (3.11)$$

Taking derivative of θ of Eq. (3.1c) yields

$$\frac{dg(\zeta)}{d\theta} = i\zeta \cdot \kappa z'(\zeta) \Phi(\zeta) - i\zeta \cdot z'(\zeta) \bar{\Phi}(\zeta) + i\bar{\zeta} \cdot z(\zeta) \bar{\Phi}'(\zeta) + i\bar{\zeta} \cdot \bar{z}'(\zeta) \bar{\Psi}(\zeta), \quad \zeta = \rho \cdot e^{i\theta} \in \omega^+ (r \leq \rho < 1) \quad (3.12)$$

Substituting Eq. (3.10) into Eq. (3.12) yields

$$\begin{aligned} \frac{dg(\zeta)}{d\theta} &= i\bar{\zeta} \cdot \left[z(\zeta) - \rho^2 \frac{z'(\zeta)}{z'(\bar{\zeta}^{-1})} z(\bar{\zeta}^{-1}) \right] \bar{\Phi}'(\zeta) + i\bar{\zeta} \bar{z}'(\zeta) \cdot \left[1 - \rho^2 \frac{z'(\zeta)}{z'(\bar{\zeta}^{-1})} \right] \bar{\Psi}(\zeta) \\ &\quad + i\zeta \cdot z'(\zeta) [\kappa \Phi(\zeta) + \Phi(\bar{\zeta}^{-1})], \quad \zeta = \rho \cdot e^{i\theta} \in \omega^+ (r \leq \rho < 1) \end{aligned} \quad (3.13)$$

Taking derivative of ζ of Eq. (3.1c) with consideration of Eq. (3.13) yields

$$\begin{aligned} \frac{dg(\zeta)}{d\zeta} &= \frac{dg(\zeta)}{d\theta} \cdot \frac{1}{i\zeta} = e^{-2i\theta} \cdot \left[z(\zeta) - \rho^2 \frac{z'(\zeta)}{z'(\bar{\zeta}^{-1})} z(\bar{\zeta}^{-1}) \right] \bar{\Phi}'(\zeta) + e^{-2i\theta} \bar{z}'(\zeta) \cdot \left[1 - \rho^2 \frac{z'(\zeta)}{z'(\bar{\zeta}^{-1})} \right] \bar{\Psi}(\zeta) \\ &\quad + z'(\zeta) [\kappa \Phi(\zeta) + \Phi(\bar{\zeta}^{-1})], \quad \zeta = \rho \cdot e^{i\theta} \in \omega^+ (r \leq \rho < 1) \end{aligned} \quad (3.14)$$

Respectively substituting Eqs. (3.11) and (3.14) into Eqs. (2.12b) and (2.12a) yields

$$\Phi^+(t) - \Phi^-(t) = 0, \quad t = e^{i\theta} \in c_{12} \quad (3.15a)$$

$$z'(t) [\kappa \Phi^+(t) + \Phi^-(t)] = 0, \quad t = e^{i\theta} \in c_{11} \quad (3.15b)$$

where $\Phi^+(t)$ and $\Phi^-(t)$ denote values of $\Phi(\zeta)$ approaching boundary c_1 from regions ω^+ and ω^- , respectively. Considering the the indefinite integrals in Eq. (3.2b), it would be more computationally convenient to transform Eq. (3.15) into the following form:

$$z'(\zeta) [\sigma_\rho(\zeta) + i\tau_{\rho\theta}(\zeta)]|_{\zeta \rightarrow t} = [z'(t)\Phi(t)]^+ - [z'(t)\Phi(t)]^- = 0, \quad t = e^{i\theta} \in c_{12} \quad (3.16a)$$

$$\frac{dg(\zeta)}{d\zeta}|_{\zeta \rightarrow t} = \kappa [z'(t)\Phi(t)]^+ + [z'(t)\Phi(t)]^- = 0, \quad t = e^{i\theta} \in c_{11} \quad (3.16b)$$

where $[z'(t)\Phi(t)]^+$ and $[z'(t)\Phi(t)]^-$ denote values of $z'(\zeta)\Phi(\zeta)$ approaching boundary c_1 from regions ω^+ and ω^- , respectively. The transformation from Eq. (3.15) to (3.16) is reasonable, because $z'(\zeta) \neq 0$ is single-valued, and would not alter the possible multi-valuedness of $\Phi(\zeta)$. Therefore, the mixed boundary conditions in Eq. (2.12) turn to a homogenous Riemann-Hilbert problem Eq. (3.16) with extra constraints of Eq. (2.12c).

4 Solution of the Riemann-Hilbert problem

4.1 Complex potential expansion

As pointed out in last section that $z'(\zeta)\Phi(\zeta)$ should be analytic within the annular region $\omega^+ \cup c_1 \cup \omega^-$ without any singularity, the general solution for the Riemann-Hilbert problem in Eq. (3.16) should satisfy the following form according to Plemelj formula [Muskhelishvili, 1966] as

$$\varphi'(\zeta) = z'(\zeta)\Phi(\zeta) = X(\zeta) \sum_{n=-\infty}^{\infty} id_n \zeta^n, \quad \zeta = \rho \cdot e^{i\theta}, \quad r \leq \rho \leq r^{-1} \quad (4.1)$$

where

$$X(\zeta) = (\zeta - e^{-i\theta_0})^{-\frac{1}{2}-i\lambda} (\zeta - e^{i\theta_0})^{-\frac{1}{2}+i\lambda}, \quad \lambda = \frac{\ln \kappa}{2\pi} \quad (4.2)$$

d_n denote coefficients to be determined, and should be real owing to the axisymmetry. The imaginary unit in front of d_n denotes that the coefficients of the sum above are pure imaginary numbers, because the geometry of the remaining geomaterial, as well as the tractions and constraints acting upon both boundaries, are all axisymmetrical about y axis. The infinite Laurent series suggest bipole $\zeta = 0$ and $\zeta = \infty$ for the annular region $r \leq \rho \leq r^{-1}$. To solve the coefficients, all items in Eq. (4.1) should be prepared into rational series. $X(\zeta)$ can be respectively expanded in regions ω^+ and ω^- using Taylor expansions as

$$X(\zeta) = \sum_{k=0}^{\infty} \alpha_k \zeta^k, \quad \zeta \in \omega^+ \quad (4.3a)$$

$$X(\zeta) = \sum_{k=1}^{\infty} \beta_k \zeta^{-k}, \quad \zeta \in \omega^- \quad (4.3b)$$

where

$$\begin{cases} \alpha_0 = -e^{-2\lambda\theta_0} \\ \alpha_1 = -e^{-2\lambda\theta_0} (\cos \theta_0 - 2\lambda \sin \theta_0) \\ \alpha_k = -e^{-2\lambda\theta_0} \cdot (-1)^k \left[\frac{a_k}{k!} + \frac{\bar{a}_k}{k!} + \sum_{l=1}^{k-1} \frac{a_l}{l!} \cdot \frac{\bar{a}_{k-l}}{(k-l)!} \right], \quad k \geq 2 \\ a_k = \prod_{l=1}^k \left(\frac{1}{2} - i\lambda - l \right) \cdot e^{ik\theta_0} \end{cases}$$

$$\begin{cases} \beta_1 = 1 \\ \beta_2 = \cos \theta_0 + 2\lambda \sin \theta_0 \\ \beta_k = (-1)^{k-1} \left[\frac{b_{k-1}}{(k-1)!} + \frac{\bar{b}_{k-1}}{(k-1)!} + \sum_{l=1}^{k-2} \frac{b_l}{l!} \cdot \frac{\bar{b}_{k-1-l}}{(k-1-l)!} \right], \quad k \geq 3 \\ b_k = \prod_{l=1}^k \left(\frac{1}{2} - i\lambda - l \right) \cdot e^{-ik\theta_0} \end{cases}$$

Last equations show that α_k and β_k are both real, which is identical to the axisymmetry of the model. The branch of $X(\zeta)$ in Eq. (4.3b) is correct, since it potentially guarantees $\lim_{\zeta \rightarrow \infty} \zeta X(\zeta) = 1$.

Substituting Eq. (4.3) into Eq. (4.1) yields

$$\varphi'(\zeta) = z'(\zeta) \Phi(\zeta) = \sum_{k=-\infty}^{\infty} iA_k \zeta^k, \quad A_k = \sum_{n=-\infty}^k \alpha_{k-n} d_n, \quad \zeta \in \omega^+ \quad (4.4a)$$

$$\varphi'(\zeta) = z'(\zeta) \Phi(\zeta) = \sum_{k=-\infty}^{\infty} iB_k \zeta^k, \quad B_k = \sum_{n=k+1}^{\infty} \beta_{n-k} d_n, \quad \zeta \in \omega^- \quad (4.4b)$$

Since $z'(\zeta) \neq 0$ for both regions ω^+ and ω^- , Eq. (4.4) can be transformed as

$$\Phi(\zeta) = \frac{(1-\zeta)^2}{-2ia} \sum_{k=-\infty}^{\infty} iA_k \zeta^k, \quad \zeta \in \omega^+ \quad (4.4a')$$

$$\Phi(\zeta) = \frac{(1-\zeta)^2}{-2ia} \sum_{k=-\infty}^{\infty} iB_k \zeta^k, \quad \zeta \in \omega^- \quad (4.4b')$$

Eqs. (4.4a) and (4.4a') should be analytic along boundary c_1 as well. Hence, Eq. (4.4a') analytically validates the foresight in Eq. (3.3) that $\Phi(\zeta)$ contains multiplier $(1 - \zeta)^2$ and is analytic within region ω . Substituting Eqs. (4.4b), (4.4a'), and (2.6b) into Eq. (3.7) yields

$$\psi'(\zeta) = z'(\zeta)\Psi(\zeta) = \sum_{k=-\infty}^{\infty} i \left[\frac{k+1}{2} (A_{k-1} - A_{k+1}) - B_{-k-2} \right] \zeta^k \quad (4.5)$$

4.2 Static equilibrium and displacement single-valuedness

Static equilibrium between the constrained ground surface and the unbalanced resultant along tunnel periphery should be satisfied in the proposed mechanical model. In the physical plane, the static equilibrium can be expressed as:

$$\int_{C_{11}} [X_o(T) + iY_o(T)] |dT| = - \oint_{C_2} [X_i(S) + iY_i(S)] |dS| \quad (4.6)$$

where $|dT|$ and $|dS|$ denote length increments along boundaries C_{11} and C_2 in the physical plane, respectively. The integral path for C_{11} is from point T_1 along ground surface towards infinity, then from infinity along ground surface towards point T_2 , so that the geomaterial always lies on the left side of the integral path. Considering the zero traction along boundary C_{12} in Eq. (2.12b), the left-hand side of Eq. (4.6) can be modified as

$$\int_{C_{11}} [X_o(T) + iY_o(T)] |dT| = \int_{C_1} [X_o(T) + iY_o(T)] |dT| = \oint_{c_1} e^{i\theta} z'(e^{i\theta}) [\sigma_\rho(e^{i\theta}) + i\tau_{\rho\theta}(e^{i\theta})] d\theta \quad (4.7)$$

where $|dT| = |z'(e^{i\theta})| \cdot |ie^{i\theta}| \cdot |d\theta| = |z'(e^{i\theta})| d\theta$ for counter-clockwise length increment in the mapping plane. Substituting Eqs. (3.16a) and (4.4) into Eq. (4.7) yields

$$\oint \left(\sum_{k=-\infty}^{\infty} A_k e^{ik\theta} - \sum_{k=-\infty}^{\infty} B_k e^{ik\theta} \right) \cdot ie^{i\theta} d\theta = 2\pi i (A_{-1} - B_{-1}) \quad (4.8)$$

On the other hand, according to Eq. (2.4), the right-hand side of Eq. (4.6) can be written as

$$-\oint_{C_2} [X_i(S) + iY_i(S)] |dS| = - \oint_{C_2} X_i(S) |dS| - i \oint_{C_2} Y_i(S) |dS| = -F_x - iF_y = -i\gamma\pi R^2 \quad (4.9)$$

The equilibrium of Eqs. (4.8) and (4.9) gives

$$A_{-1} - B_{-1} = -\frac{\gamma R^2}{2} \quad (4.10)$$

In the physical plane, the displacement single-valuedness of geomaterial owing to the displacement boundary in Eq. (2.12a) should be guaranteed and verified. Substituting Eqs. (4.4a), (4.4a'), and (4.5) into Eq. (3.1c) yields

$$\begin{aligned} g(\zeta) &= \kappa \int z'(\zeta)\Phi(\zeta) d\zeta - z(\zeta)\overline{\Phi(\zeta)} - \int \overline{z'(\zeta)\Psi(\zeta)} d\bar{\zeta} + iC_0 \\ &= i(\kappa A_{-1} + B_{-1}) \text{Ln}e^{i\theta} + i(\kappa A_{-1} - B_{-1}) \ln \rho + \text{single valued items} \end{aligned} \quad (4.11)$$

where Ln denotes the multi-valued natural logarithm sign, C_0 denotes the integral constant, which should be real due to symmetry, to ensure $g(1) = 0$ to satisfy the displacement boundary condition in Eq. (2.12a). The displacement single-valuedness of Eq. (4.11) requires that the multi-valued natural logarithm item should vanish. Thus, we have

$$\kappa A_{-1} + B_{-1} = 0 \quad (4.12)$$

Eq. (4.12) ensures displacement single-valuedness of the geomaterial. Eqs. (4.10) and (4.12) give

$$\begin{cases} A_{-1} = \frac{-\gamma R^2}{2(1 + \kappa)} \\ B_{-1} = \frac{\kappa\gamma R^2}{2(1 + \kappa)} \end{cases} \quad (4.13)$$

The deduction above indicates that Eqs. (4.10) and (4.12) are free from conformal mapping. Such a result is reasonable, since the resultant equilibrium and displacement single-valuedness should always be satisfied for arbitrary doubly-connected region of the mixed boundary conditions in Eq. (2.12). The integral constant C_0 could be determined in a later stage.

4.3 Traction boundary condition along tunnel periphery

Traction boundary condition in Eq. (2.12c) should be also satisfied to uniquely determine the unknown coefficients d_n in Eq. (4.1). However, the original form in Eq. (2.12c) would cause computational difficulties, and corresponding path integral form can be used instead. To use the path integral along the boundary C_2 in the physical plane, as well as along the boundary c_2 in the mapping plane, we denote the starting point by A and an arbitrary integral point by B in the physical plane, and the mapping points of these two points in the mapping plane are respectively denoted by a and b . Note that point B is always clockwise to point A in both the physical and mapping planes, so that the integral path would always keep the geomaterial on the left hand.

The first equilibrium in Eq. (2.12c) can be equivalently modified in the following path integral form as

$$-i \int_A^B [X_i(S) + iY_i(S)] \cdot |dS| = -i \int_a^b e^{i\theta} \frac{z'(s)}{|z'(s)|} [\sigma_\rho(s) + i\tau_{\rho\theta}(s)] \cdot |z'(s)| \cdot |ds| = \int_a^b z'(s) [\sigma_\rho(s) + i\tau_{\rho\theta}(s)] ds \quad (4.14)$$

where $|ds| = |rde^{i\theta}| = r|d\theta| = -rd\theta = -ds$ for clockwise length increment in mapping plane. Simultaneously, the second equilibrium in Eq. (2.12c) can be modified in the following integral form as

$$-i \int_A^B [X_i(S) + iY_i(S)] \cdot |dS| = i \int_A^B \left(-k_0 \gamma y \frac{dy}{dS} + i\gamma y \frac{dx}{dS} \right) dS = -ik_0 \gamma \int_A^B y dy - \gamma \int_A^B y dx \quad (4.15)$$

where $|dS| = R|d\vartheta| = -Rd\vartheta = -dS$ for clockwise length increment in physical plane, similar to Eq. (2.4).

As long as the difference between the indefinite integrals in Eqs. (4.14) and (4.15) is a constant, Eq. (2.12c) would be satisfied. Both Eqs. (4.14) and (4.15) should be prepared into rational series in the mapping plane. Substituting Eq. (3.1b) into Eq. (4.14) yields

$$\begin{aligned} \int_a^b z'(s) [\sigma_\rho(s) + i\tau_{\rho\theta}(s)] ds &= \int_a^b \varphi'(s) ds + \frac{z(s)}{z'(s)} \overline{\varphi'(s)} + \int_a^b \overline{\psi'(s)} d\bar{s} \\ &= \frac{1}{-2i(1-re^{i\theta})} \sum_{k=-\infty}^{\infty} \left[\begin{array}{l} r^{-k+2} A_{-k+1} + (1-2r^2)r^{-k} A_{-k} \\ +(r^2-2)r^{-k} A_{-k-1} + r^{-k} A_{-k-2} \end{array} \right] e^{ik\theta} \\ &\quad + i \sum_{k=1}^{\infty} \left[\frac{r^k}{k} A_{k-1} - \frac{r^{-k}}{2} (A_{-k-2} - A_{-k}) + \frac{r^{-k}}{-k} B_{k-1} \right] e^{ik\theta} \\ &\quad + i \sum_{k=1}^{\infty} \left[\frac{r^{-k}}{-k} A_{-k-1} - \frac{r^k}{2} (A_{k-2} - A_k) + \frac{r^k}{k} B_{-k-1} \right] e^{-ik\theta} \\ &\quad + i(A_{-1} + B_{-1}) \ln r + i(A_{-1} - B_{-1}) \ln e^{i\theta} + iC_a \end{aligned} \quad (4.14a)$$

where C_a denotes the integral constant to be determined and should be real due to symmetry. Considering the backward conformal mapping in Eq. (2.10b), the real variables x and y along boundary C_2 in Eq. (4.15) can be written as

$$x = -\frac{ia}{2} \left(\frac{1+re^{i\theta}}{1-re^{i\theta}} - \frac{e^{i\theta}+r}{e^{i\theta}-r} \right) \quad (4.16a)$$

$$y = -\frac{a}{2} \left(\frac{1+re^{i\theta}}{1-re^{i\theta}} + \frac{e^{i\theta}+r}{e^{i\theta}-r} \right) \quad (4.16b)$$

$$dx = -iar \left[\frac{1}{(1-re^{i\theta})^2} + \frac{1}{(e^{i\theta}-r)^2} \right] de^{i\theta} \quad (4.16c)$$

Substituting Eq. (4.16) into Eq. (4.15) with notation of $\frac{ar}{1-r^2} = \frac{R}{2}$ yields

$$\begin{aligned} -ik_0\gamma \int_A^B ydy - \gamma \int_A^B ydx = & -\frac{ik_0\gamma a^2(1-r^2)^2 e^{2i\theta}}{2(1-re^{i\theta})^2(e^{i\theta}-r)^2} - \frac{i\gamma a^2}{2(1-re^{i\theta})^2} + \frac{i\gamma a^2 r^2}{2(e^{i\theta}-r)^2} \\ & + \frac{i\gamma a R}{2(e^{i\theta}-r)} - \frac{i\gamma a r R}{2(1-re^{i\theta})} + \frac{i\gamma R^2}{2} \ln \frac{1-re^{i\theta}}{1-re^{-i\theta}} - \frac{i\gamma R^2}{2} \ln e^{i\theta} \end{aligned} \quad (4.15a)$$

According to Eqs. (4.14) and (4.15), Eqs. (4.14a) and (4.15a) should be equal. To guarantee such a requirement, the multi-valued components of $\ln e^{i\theta}$ should be eliminated simultaneously, and we again obtain Eq. (4.10). The deduction above further analytically emphasizes the mechanical fact that stress and traction in the geomaterial should be single-valued.

Eqs. (4.14a) and (4.15a) should be equal, however, owing to the denominator $-2i(1-re^{i\theta})$, the equilibrium is not in rational form to facilitate coefficient comparisons, thus, we should modify the equilibrium. Eqs. (4.14a) can be modified as

$$\begin{aligned} & -2i(1-re^{i\theta}) \left[\int_a^b \varphi'(s)ds + \frac{z(s)}{z'(s)} \overline{\varphi'(s)} + \int_a^b \overline{\psi'(s)}d\bar{s} \right] \\ & = \sum_{k=1}^{\infty} \left[\frac{2r^{-k}}{-k} A_{-k-1} - \frac{2r^{-k}}{-k-1} A_{-k-2} + \frac{2r^k}{k} B_{-k-1} - \frac{2r^{k+2}}{k+1} B_{-k-2} + 2(1-r^2)r^k(A_k - A_{k-1}) \right] e^{-ik\theta} \\ & + \sum_{k=2}^{\infty} \left[\frac{2r^k}{k} A_{k-1} - \frac{2r^k}{k-1} A_{k-2} + \frac{2r^{-k}}{-k} B_{k-1} - \frac{2r^{-k+2}}{-k+1} B_{k-2} + 2(1-r^2)r^{-k}(A_{-k} - A_{-k-1}) \right] e^{ik\theta} \\ & + \left[2(B_0 - r^2 A_0) + 2(1-r^2)A_{-2} + 2(r^2 - 1)A_{-1} + r^2 \tilde{C}_a \right] (-r^{-1}e^{i\theta}) \\ & + \left[2(1-r^2)A_0 + 2(A_{-2} - r^2 B_{-2}) + 2(r^2 - 1)A_{-1} + \tilde{C}_a \right] \end{aligned} \quad (4.14b)$$

where

$$\tilde{C}_a = -(A_0 - A_{-2}) + 2(A_{-1} + B_{-1}) \ln r + 2C_a$$

The coefficients in Eq. (4.14b) would degenerate to the ones in Refs Verruijt [1997b], when we replace the unbalanced resultant along tunnel periphery by a balanced traction and cancel the far-field displacement constraint along ground surface. The degeneration and comparison details can be found in Appendix A. Similarly, Eq. (4.15a) can be modified as

$$-2i(1-re^{i\theta}) \left(-ik_0\gamma \int_A^B ydy - \gamma \int_A^B ydx \right) = \sum_{k=1}^{\infty} E_{-k} e^{-ik\theta} + \sum_{k=2}^{\infty} E_k e^{ik\theta} + E_1 e^{i\theta} + E_0 \quad (4.15b)$$

where E_k can be found in Appendix B. The equilibriums of coefficients between Eqs. (4.14b) and (4.15b) with some slight modification respectively give

$$A_{-k-1} - A_{-k-2} = -\frac{1}{k+1} A_{-k-2} + r^{2k} B_{-k-1} - \frac{k}{k+1} r^{2k+2} B_{-k-2} + k(1-r^2)r^{2k}(A_k - A_{k-1}) - \frac{k}{2} r^k E_{-k}, \quad k \geq 1 \quad (4.17a)$$

$$B_{k-1} = \frac{k}{k-1} r^2 B_{k-2} + r^{2k} A_{k-1} - \frac{k}{k-1} r^{2k} A_{k-2} + k(1-r^2)(A_{-k} - A_{-k-1}) - \frac{k}{2} r^k E_k, \quad k \geq 2 \quad (4.17b)$$

$$2B_0 - 3r^2 A_0 + (2-r^2)A_{-2} + 2r^2 C_a = -rE_1 + 2(1-r^2)A_{-1} - 2r^2(A_{-1} + B_{-1}) \ln r \quad (4.18a)$$

$$(1-2r^2)A_0 + 3A_{-2} - 2r^2 B_{-2} + 2C_a = E_0 + 2(1-r^2)A_{-1} - 2(A_{-1} + B_{-1}) \ln r \quad (4.18b)$$

4.4 Solution

With Eqs. (4.17), (4.18), and (4.13), we can solve d_n using an approximate method below. For better convergence, we substitute Eq. (4.17a) into Eq. (4.17b), and Eq. (4.17) can be further modified as

$$\begin{aligned} A_{-k} &= \frac{k-1}{k} A_{-k-1} + r^{2k-2} B_{-k} - \frac{k-1}{k} r^{2k} B_{-k-1} \\ &\quad + (k-1)(1-r^2)r^{2k-2}(A_{k-1} - A_{k-2}) - \frac{k-1}{2} r^{k-1} E_{-k+1}, \quad k \geq 2 \end{aligned} \quad (4.19a)$$

$$\begin{aligned} B_k &= \frac{k+1}{k} r^2 B_{k-1} + r^{2k+2} A_k - \frac{k+1}{k} r^{2k+2} A_{k-1} - (1-r^2) A_{-k-2} \\ &\quad + (k+1)(1-r^2)r^{2k} B_{-k-1} - k(1-r^2)r^{2k+2} B_{-k-2} \\ &\quad + k(k+1)(1-r^2)^2 r^{2k} (A_k - A_{k-1}) - \frac{k(k+1)}{2} (1-r^2) r^k E_{-k} - \frac{k+1}{2} r^{k+1} E_{k+1}, \quad k \geq 1 \end{aligned} \quad (4.19b)$$

Using Eq. (4.4), the left-hand sides of Eq. (4.19) can be expanded as

$$\begin{aligned} \sum_{n=k}^{\infty} \alpha_{n-k} d_{-n} &= \frac{k-1}{k} A_{-k-1} + r^{2k-2} B_{-k} - \frac{k-1}{k} r^{2k} B_{-k-1} \\ &\quad + (k-1)(1-r^2)r^{2k-2}(A_{k-1} - A_{k-2}) - \frac{k-1}{2} r^{k-1} E_{-k+1}, \quad k \geq 2 \end{aligned} \quad (4.20a)$$

$$\begin{aligned} \sum_{n=k+1}^{\infty} \beta_{n-k} d_n &= \frac{k+1}{k} r^2 B_{k-1} + r^{2k+2} A_k - \frac{k+1}{k} r^{2k+2} A_{k-1} - (1-r^2) A_{-k-2} \\ &\quad + (k+1)(1-r^2)r^{2k} B_{-k-1} - k(1-r^2)r^{2k+2} B_{-k-2} \\ &\quad + k(k+1)(1-r^2)^2 r^{2k} (A_k - A_{k-1}) - \frac{k(k+1)}{2} (1-r^2) r^k E_{-k} - \frac{k+1}{2} r^{k+1} E_{k+1}, \quad k \geq 1 \end{aligned} \quad (4.20b)$$

Eqs. (4.20a) and (4.20b) constrain d_{-n} ($n \geq 2$) and d_n ($n \geq 2$), respectively, while d_{-1} , d_0 , and d_1 are not constrained yet. Thus, Eqs. (4.18) and (4.13) should be used and can be expanded as

$$I_{-1} d_{-1} + I_0 d_0 + I_1 d_1 + 2r^2 C_a = - \sum_{n=2}^{\infty} I_{-n} d_{-n} - \sum_{n=2}^{\infty} I_n d_n + I' \quad (4.21a)$$

$$J_{-1} d_{-1} + J_0 d_0 + J_1 d_1 + 2C_a = - \sum_{n=2}^{\infty} J_{-n} d_{-n} - \sum_{n=2}^{\infty} J_n d_n + J' \quad (4.21b)$$

$$\alpha_0 d_{-1} = - \sum_{n=2}^{\infty} \alpha_{-1+n} d_{-n} + \frac{-\gamma R^2}{2(1+\kappa)} \quad (4.21c)$$

$$\beta_1 d_0 + \beta_2 d_1 = - \sum_{n=2}^{\infty} \beta_{n+1} d_n + \frac{\kappa\gamma R^2}{2(1+\kappa)} \quad (4.21d)$$

where

$$\left\{ \begin{array}{l} I_n = 2\beta_n, \quad n \geq 1 \\ I_0 = -3r^2\alpha_0 \\ I_{-1} = -3r^2\alpha_1 \\ I_{-n} = (2-r^2)\alpha_{-2+n} - 3r^2\alpha_n, \quad n \geq 2 \\ I' = \frac{-\gamma R^2}{1+\kappa} (1-r^2) + \frac{1-\kappa}{1+\kappa} \gamma R^2 r^2 \ln r - r E_1 \end{array} \right.$$

$$\begin{cases} J_n = -2r^2\beta_{n+2}, & n \geq 1 \\ J_0 = (1-2r^2)\alpha_0 - 2r^2\beta_2 \\ J_{-1} = (1-2r^2)\alpha_1 - 2r^2\beta_1 \\ J_{-n} = (1-2r^2)\alpha_n + 3\alpha_{-2+n}, & n \geq 2 \\ J' = \frac{-\gamma R^2}{1+\kappa} (1-r^2) + \frac{1-\kappa}{1+\kappa} \gamma R^2 \ln r + E_0 \end{cases}$$

Eq. (4.21) contains four linear equations on four variables (d_{-1} , d_0 , d_1 , and C_a). Thus, the linear system on d_k and C_a composed of Eqs. (4.20) and (4.21) are definite, as long as the values of A_k and B_k are determined.

Assume that d_n and C_a can be written as

$$d_n = \sum_{q=0}^{\infty} d_n^{(q)}, \quad n \in \mathbf{Z} \quad (4.22a)$$

$$C_a = \sum_{q=0}^{\infty} C_a^{(q)} \quad (4.22b)$$

Then the initial values of $d_{-n}^{(0)} (n \geq 2)$ and $d_n^{(0)} (n \geq 2)$ can be determined by the following linear system based on Eq. (4.20) as

$$\sum_{n=k}^{\infty} \alpha_{-k+n} d_{-n}^{(0)} = -\frac{k-1}{2} r^{k-1} E_{-k+1}, \quad k \geq 2 \quad (4.23a)$$

$$\sum_{n=k+1}^{\infty} \beta_{n-k} d_n^{(0)} = -\frac{k(k+1)}{2} (1-r^2) r^k E_{-k} - \frac{k+1}{2} r^{k+1} E_{k+1}, \quad k \geq 1 \quad (4.23b)$$

Then the initial value of $d_{-1}^{(0)}$, $d_0^{(0)}$, $d_1^{(0)}$, and $C_a^{(0)}$ can be determined by the following linear system based on Eq. (4.21) as

$$I_{-1} d_{-1}^{(0)} + I_0 d_0^{(0)} + I_1 d_1^{(0)} + 2r^2 C_a^{(0)} = -\sum_{n=2}^{\infty} I_{-n} d_{-n}^{(0)} - \sum_{n=2}^{\infty} I_n d_n^{(0)} + I' \quad (4.24a)$$

$$J_{-1} d_{-1}^{(0)} + J_0 d_0^{(0)} + J_1 d_1^{(0)} + 2C_a^{(0)} = -\sum_{n=2}^{\infty} J_{-n} d_{-n}^{(0)} - \sum_{n=2}^{\infty} J_n d_n^{(0)} + J' \quad (4.24b)$$

$$\alpha_0 d_{-1}^{(0)} = -\sum_{n=2}^{\infty} \alpha_{-1+n} d_{-n}^{(0)} + \frac{-\gamma R^2}{2(1+\kappa)} \quad (4.24c)$$

$$\beta_1 d_0^{(0)} + \beta_2 d_1^{(0)} = -\sum_{n=2}^{\infty} \beta_{n+1} d_n^{(0)} + \frac{\kappa \gamma R^2}{2(1+\kappa)} \quad (4.24d)$$

Eq. (4.24) indicates that $d_{-1}^{(0)}$, $d_0^{(0)}$, $d_1^{(0)}$, and $C_a^{(0)}$ are dependent on $d_{-n}^{(0)} (n \geq 2)$ and $d_n^{(0)} (n \geq 2)$ solved via Eq. (4.23).

With the initial values in Eqs. (4.23) and (4.24), for iteration rep $q \geq 0$, the coefficients of $\varphi(\zeta)$ in Eq. (4.4) can be computed as

$$A_k^{(q)} = \sum_{n=-\infty}^k \alpha_{k-n} d_n^{(q)} \quad (4.25a)$$

$$B_k^{(q)} = \sum_{n=k+1}^{\infty} \beta_{n-k} d_n^{(q)} \quad (4.25b)$$

Then for the next iteration rep $q + 1$, $d_{-n}^{(q+1)}$ ($q \geq 0, n \geq 2$) and $d_n^{(q+1)}$ ($q \geq 0, n \geq 2$) can be determined via the following linear system based on Eq. (4.20) as

$$\begin{aligned} \sum_{n=k}^{\infty} \alpha_{n-k} d_{-n}^{(q+1)} &= \frac{k-1}{k} A_{-k-1}^{(q)} + r^{2k-2} B_{-k}^{(q)} - \frac{k-1}{k} r^{2k} B_{-k-1}^{(q)} \\ &\quad + (k-1)(1-r^2) r^{2k-2} (A_{k-1}^{(q)} - A_{k-2}^{(q)}), \quad k \geq 2 \end{aligned} \quad (4.26a)$$

$$\begin{aligned} \sum_{n=k+1}^{\infty} \beta_{n-k} d_n^{(q+1)} &= \frac{k+1}{k} r^2 B_{k-1}^{(q)} + r^{2k+2} A_k^{(q)} - \frac{k+1}{k} r^{2k+2} A_{k-1}^{(q)} - (1-r^2) A_{k-2}^{(q)} \\ &\quad + (k+1)(1-r^2) r^{2k} B_{-k-1}^{(q)} - k(1-r^2) r^{2k+2} B_{-k-2}^{(q)} \\ &\quad + k(k+1)(1-r^2)^2 r^{2k} (A_k^{(q)} - A_{k-1}^{(q)}), \quad k \geq 1 \end{aligned} \quad (4.26b)$$

Subsequently, $d_{-1}^{(q+1)}$, $d_0^{(q+1)}$, $d_1^{(q+1)}$, and $C_a^{(q+1)}$ ($q \geq 0$) can be determined via the following linear system based on Eq. (4.21) as

$$I_{-1} d_{-1}^{(q+1)} + I_0 d_0^{(q+1)} + I_1 d_1^{(q+1)} + 2r^2 C_a^{(q+1)} = - \sum_{n=2}^{\infty} I_{-n} d_{-n}^{(q+1)} - \sum_{n=2}^{\infty} I_n d_n^{(q+1)} \quad (4.27a)$$

$$J_{-1} d_{-1}^{(q+1)} + J_0 d_0^{(q+1)} + J_1 d_1^{(q+1)} + 2C_a^{(q+1)} = - \sum_{n=2}^{\infty} J_{-n} d_{-n}^{(q+1)} - \sum_{n=2}^{\infty} J_n d_n^{(q+1)} \quad (4.27b)$$

$$\alpha_0 d_{-1}^{(q+1)} = - \sum_{n=2}^{\infty} \alpha_{-1+n} d_{-n}^{(q+1)} \quad (4.27c)$$

$$\beta_1 d_0^{(q+1)} + \beta_2 d_1^{(q+1)} = - \sum_{n=2}^{\infty} \beta_{n+1} d_n^{(q+1)} \quad (4.27d)$$

Eq. (4.27) indicates that $d_{-1}^{(q+1)}$, $d_0^{(q+1)}$, $d_1^{(q+1)}$, and $C_a^{(q+1)}$ ($q \geq 0$) are dependent on $d_{-n}^{(q+1)}$ ($n \geq 2, q \geq 0$) and $d_n^{(q+1)}$ ($n \geq 2, q \geq 0$) solved in Eq. (4.26). Then we can set $q := q + 1$ to continue the iteration, until

$$\max |d_n^{(q+1)}| \leq \varepsilon$$

is reached, where ε is a small numeric, $\varepsilon = 10^{-16}$ for instance, which is the default machine accuracy of double precision of the programming code **fortran**.

4.5 Solution convergence and numerical truncation

The approximate solution consists of the initial value determination phase in Eqs. (4.23) and (4.24) and the iteration phase in Eqs. (4.26) and (4.27). Obviously, the latter determines the solution convergence. As long as the absolute values of the coefficients in front of A_k and B_k in Eq. (4.26) are less than 1, the magnitudes of $d_n^{(q)}$ would approach zero as iteration procedes (q increases). Henceforth, we should examine the value ranges of these coefficients in front of A_k and B_k in Eq. (4.26).

It is common in shallow tunnel engineering that tunnel buried depth h is 2 times larger than tunnel radius R ($h \geq 2R$), which leads to $r \leq (2 + \sqrt{3})^{-1}$ according to Eq. (2.11). It can be easily verified that such a range of r would guarantee that the absolute values of all coefficients in front of A_k and B_k in Eq. (4.26) are less than 1, and the computation is so plain that it is not necessary to be expanded here. Therefore, such a range of r would further guarantee the convergence of the iteration procedure in Eqs. (4.23)-(4.27). In other words, in the iteration procedure in Eqs. (4.23)-(4.27), as q increases, the magnitudes of $d_n^{(q)}$ would approach zero.

To obtain numerical solution in practical computation, we have to truncate the infinite bilateral series of d_n in Eq. (4.1) into $2N + 1$ items ($-N \leq n \leq N$), and the coefficients in Eq. (4.4) would correspondingly turn to the following form:

$$\begin{cases} A_k = \sum_{n=-N}^k \alpha_{k-n} d_n \\ B_k = \sum_{n=k+1}^N \beta_{n-k} d_n \end{cases}$$

Subsequently, all the equations in the Section 4.4 would turn to finite, as well as the E_k series in Eq. (4.15b). No matter in the initial value determination phase in Eqs. (4.23) and (4.24), or in the iteration phase in Eqs. (4.26) and (4.27), three linear equation system sets can be established: (1) Set 1: Eqs. (4.23a) and (4.26a), which independently determine $d_{-n}^{(q)}$ ($2 \leq n \leq N, q \geq 0$); (2) Set 2: Eqs. (4.23b) and (4.26b), which independently determine $d_n^{(q)}$ ($2 \leq n \leq N, q \geq 0$); (3) Set 3: Eqs. (4.24) and (4.27), which further determine $d_1^{(q)}, d_0^{(q)}, d_{-1}^{(q)}$, and $C_a^{(q)}$ ($q \geq 0$) for completion. The three sets can be written into the following form:

$$\mathbf{A}_l \cdot \mathbf{x}_l = \mathbf{b}_l, \quad l = 1, 2, 3 \quad (4.28)$$

where \mathbf{A}_l , \mathbf{x}_l , and \mathbf{b}_l respectively denote the coefficient matrix, the variable vector, and the constant vector for sets of linear systems $l = 1, 2, 3$. The coefficient matrices of linear system sets 1 and 2 can be expanded below:

$$\mathbf{A}_1(i, j) = \alpha_{j-i}, \quad 1 \leq i \leq j \leq N - 1 \quad (4.29a)$$

$$\mathbf{A}_2(i, j) = \beta_{j-i+1}, \quad 1 \leq i \leq j \leq N - 1 \quad (4.29b)$$

The other components of these three linear system sets are plain in Eqs. (4.23), (4.24), (4.26), and (4.27).

With the coefficient matrices in Eq. (4.29), we can explain the reason of applying the approximate solution. Intuitively, it seems that applying the approximate solution above is very indirect and complicated, since the problem is definitely a linear elastic one and could be solved via a more direct solution containing only one single linear system, instead of such a great deal of linear systems piled in iteration. Indeed, such a problem can be solved via one single linear system, but the numerical stability can not be theoretically guaranteed. When dealing with solution of linear system, we should consider numerical stability as well, which is greatly related to condition number of the coefficient matrix. For the direct solution, the condition number would be very large, since the elements would contain both positive and negative powers of r , as can be seen in the coefficients in Eq. (4.14b). Then the condition number of the coefficient matrix measured by 2-norm would be very large, and would make the solution of the direct method potentially unstable, and might cause great error. In contrast, Eqs. (4.24), (4.27), and (4.29) show that the condition numbers of the coefficient matrices \mathbf{A}_l ($l = 1, 2, 3$) would be small, which is further verified in the numerical verification and case discussions.

5 Stress and displacement in geomaterial

The solution of d_n gives A_k and B_k in Eq. (4.4) to reach $\varphi(\zeta)$ in Eq. (4.4) and $\varPhi(\zeta)$ in Eq. (4.4a'), as well as $\psi(\zeta)$ in Eq. (4.5). The stress and displacement components within the annulus ω can be obtained via Eq. (3.1) as

$$\sigma_\theta(\zeta) + \sigma_\rho(\zeta) = 4\Re \left[\frac{(1-\zeta)^2}{-2a} \sum_{k=-\infty}^{\infty} \zeta^k A_k \right], \quad \zeta = \rho \cdot e^{i\theta} \in \omega \quad (5.1a)$$

$$\begin{aligned} \sigma_\rho(\zeta) + i\tau_{\rho\theta}(\zeta) = & \sum_{k=-\infty}^{\infty} \left[\frac{(1-\bar{\zeta})^2}{-2a} \bar{\zeta}^k + \frac{k+2}{\sigma^2} \frac{(1-\zeta)^2}{-4a} \bar{\zeta}^{k+1} + \frac{k}{\sigma^2} \frac{(1-\zeta)^2}{4a} \bar{\zeta}^{k-1} \right. \\ & \left. + \frac{1-\zeta^2}{-2a} \frac{1-\bar{\zeta}}{\sigma^2} \bar{\zeta}^k + \frac{1-\zeta^2}{4a} \frac{(1-\bar{\zeta})^2}{\sigma^2} k \bar{\zeta}^{k-1} + \frac{(1-\zeta)^2}{-2a} \bar{\zeta}^k \right] A_k \\ & + \sum_{k=-\infty}^{\infty} \frac{(1-\zeta)^2}{2a\sigma^2} \bar{\zeta}^{-k-2} B_k \end{aligned} \quad (5.1b)$$

$$\begin{aligned} g(\zeta) = 2G[u(\zeta) + iv(\zeta)] = & i \sum_{k=1}^{\infty} \left\{ \kappa A_{k-1} \frac{\zeta^k}{k} + \left[\frac{1}{2}(A_{k-2} - A_k) - \frac{B_{-k-1}}{k} \right] \bar{\zeta}^k \right\} \\ & + i \sum_{k=1}^{\infty} \left\{ \kappa A_{-k-1} \frac{\zeta^{-k}}{-k} + \left[\frac{1}{2}(A_{-k-2} - A_{-k}) - \frac{B_{k-1}}{-k} \right] \bar{\zeta}^{-k} \right\}, \quad \zeta = \rho \cdot e^{i\theta} \in \omega \\ & - i \frac{1+\zeta}{2} \frac{(1-\bar{\zeta})^2}{1-\zeta} \sum_{k=-\infty}^{\infty} A_k \bar{\zeta}^k + i(\kappa A_{-1} - B_{-1}) \ln \rho + iC_0 \end{aligned} \quad (5.1c)$$

where $\sigma_\rho(\zeta)$, $\sigma_\theta(\zeta)$, and $\tau_{\rho\theta}(\zeta)$ denote radial, hoop, and tangential stress components in the unit annulus, respectively; $u(\zeta)$ and $v(\zeta)$ denote horizontal and vertical displacement components in the unit annulus, respectively.

When $\rho = 1$, the displacement in Eq. (5.1c) would turn to

$$\begin{aligned} g(e^{i\theta}) = & i \sum_{k=1}^{\infty} \left\{ \kappa A_{k-1} \frac{e^{ik\theta}}{k} + \left[\frac{1}{2}(A_{k-2} - A_k) - \frac{B_{-k-1}}{k} \right] e^{-ik\theta} \right\} \\ & + i \sum_{k=1}^{\infty} \left\{ \kappa A_{-k-1} \frac{e^{-ik\theta}}{-k} + \left[\frac{1}{2}(A_{-k-2} - A_{-k}) - \frac{B_{k-1}}{-k} \right] e^{ik\theta} \right\}, \quad \theta \in [0, 2\pi) \\ & - i \frac{1 - e^{2i\theta}}{2e^{2i\theta}} \sum_{k=-\infty}^{\infty} A_k e^{-ik\theta} + iC_0 \end{aligned} \quad (5.2)$$

Then the undetermined coefficient C_0 in Eq. (4.11) can be determined when $\theta = 0$ in Eq. (5.2) as

$$C_0 = - \sum_{k=1}^{\infty} \left[\kappa \frac{A_{k-1}}{k} + \frac{1}{2}(A_{k-2} - A_k) - \frac{B_{-k-1}}{k} \right] - \sum_{k=1}^{\infty} \left[\kappa \frac{A_{-k-1}}{-k} + \frac{1}{2}(A_{-k-2} - A_{-k}) - \frac{B_{k-1}}{-k} \right] \quad (5.3)$$

Eq. (5.2) indicates that the displacement components are zero, when $\zeta = 1$, instead of infinity in Refs Strack [2002], Strack and Verruijt [2002], Lu et al. [2016], Zeng et al. [2019], Lin et al. [2020] mentioned in Section 1. Till now, we can say that the displacement singularity has been cancelled.

Due to the abrupt change of boundary conditions near polar points $(1, -\theta_0)$ and $(1, \theta_0)$ in Eqs. (2.12a) and (2.12b), the Gibbs phenomena would occur in Eqs. (5.1) and (5.2), and cause oscillations of the stress and displacement components. To weaken the influence of the Gibbs phenomena, the Lanczos filtering technique is applied [Lanczos, 1956, Singh and Bhandakkar, 2019, Chawde and Bhandakkar, 2021]. To be specific, all A_k and B_k in Eqs. (5.1) and (5.3) are replaced by $L_k \cdot A_k$ and $L_k \cdot B_k$, where L_k denote the Lanczos filtering parameters, and can be expressed as

$$L_k = \begin{cases} 1, & k = 0 \\ \sin\left(\frac{k}{N}\pi\right) / \left(\frac{k}{N}\pi\right), & \text{otherwise} \end{cases} \quad (5.4)$$

With the bidirectional conformal mappings, the stress and displacement components in the unit annulus can be backwardly mapped onto the ones in the geomaterial in the lower half plane:

$$\begin{cases} \sigma_y(z) + \sigma_x(z) = \sigma_\theta(\zeta) + \sigma_\rho(\zeta) \\ \sigma_y(z) - \sigma_x(z) + 2i\tau_{xy}(z) = [\sigma_\theta(\zeta) - \sigma_\rho(\zeta) + 2i\tau_{\rho\theta}(\zeta)] \cdot \frac{\bar{\zeta} z'(\zeta)}{\zeta z'(\zeta)} \end{cases} \quad (5.5a)$$

$$u(z) + iv(z) = u(\zeta) + iv(\zeta) \quad (5.5b)$$

where $\sigma_x(z)$, $\sigma_y(z)$, and $\tau_{xy}(z)$ denote the horizontal, vertical, and shear stress components due to excavation in the lower half plane, respectively; $u(z)$ and $v(z)$ denote horizontal and vertical displacement components in the lower half plane, respectively. The final stress field within geomaterial is the sum of Eqs. (2.1) and (5.5a). Till now, the stress and displacement distributions in the geomaterial region Ω are obtained, and our problem is solved.

6 Case verification

In this section, we use numerical cases to illustrate the necessity of Lanczos filtering in Eq. (5.4), the convergence of the proposed solution in this study, and the comparisons between the solution in this study and an existing analytic solution for verification. The parameters in Table 1 are shared in all the following numerical cases in this study, while the free ground surface length x_0 is not included, since it is changable and would greatly affect the solution convergence. The geomaterial is set to be plane-strain ($\kappa = 3 - 4\nu$). All numerical cases are realized in the programming code `fortran` of `gcc-13.1.1`. The condition numbers of the coefficient matrices in all numerical cases are computed via `dgesvd` package of `lapack-3.11.0`, and the linear systems in all numerical cases are solved via `dgesv` package of `lapack-3.11.0`. All the figures are constructed via `gnuplot-5.4`. According to GNU General Public License, all the source codes in the numerical cases are released in author Luobin Lin's github repository github.com/luobinlin987/eliminate-shallow-tunnel-displacement-singularity.

The condition numbers of all the iterative linear systems in the numerical cases for the propose solution below are all less than 10^2 after computation, indicating that the solutions of the linear systems for the proposed solution in this study are numerically stable. Moreover, the iterative reps of all the numerical cases below are less than 30, indicating that the convergence of the iteration procedure in Eqs. (4.22)-(4.27) is very fast. The time cost of each numerical case is less than 0.5 sec.

R (m)	h/R	γ (kN/m ³)	k_0	E (MPa)	ν	N
5	2	20	0.8	20	0.3	50

Table 1: Parameters in numerical cases

6.1 Lanczos filtering

We first illustrate the neccessity of the Lanczos filtering in Eq. (5.4). The partially free ground surface length is selected as $x_0/h = 1$ for better demonstration, since a large x_0 would make the displacement constraint arc in the mapping plane too small, referring to the equation $\theta_0 = -i \ln \frac{x_0+ia}{x_0-ia}$ mentioned in Section 2.3 and arc $\widehat{t_1 t_2}$ Fig. 3b. Substituting the parameters in Table 1 and $x_0/h = 1$ into the solution in this study, we obtain the stress and displacement components

along ground surface in the mapping plane when using the Lanczos filtering in Eq. (5.4) or not, as shown in Fig. 4, where the abbreviation *LF* in the figure denotes Lanczos filtering.

As mentioned in Section 5, stress and displacement would show obvious oscillations of Gibbs phenomena due to abrupt change of boundary condition along ground surface. The results in Fig. 4 may serve as a strong evidence of the Gibbs phenomena along the ground surface, and also indicates that the Lanczos filtering is necessary to reduce the Gibbs phenomena. It should be addressed that the Gibbs phenomena *can not be fully eliminated*, but can only be greatly reduced by the Lanczos filtering in Eq. (5.4).

6.2 Solution convergence

Now we illustrate the convergence of the solution proposed in this study. In tunnel engineering, the ground surface is generally assumed free from any traction [Lin et al., 2020, Lu et al., 2019, Zeng et al., 2019, Lu et al., 2016, Verruijt and Strack, 2008, Verruijt, 1997b,a]. In the solution in this study, the ground surface between points T_1 and T_2 is free from traction, which is identical to the assumptions in the studies mentioned above. What is different from these studies is that the ground surface outside of points T_1 and T_2 is displacement-constrained, which is different from the assumptions [Lin et al., 2020, Lu et al., 2019, Zeng et al., 2019, Lu et al., 2016, Verruijt and Strack, 2008, Verruijt, 1997b,a].

Due to boundary effect, we should expect that as the horizontal coordinates of points T_1 and T_2 get larger, in other words, the absolute value of x_0 gets larger, we should observe convergence of all stress and displacement components. To validate such an expectation, we should substitute the parameters in Table 1 and different values of x_0/h into the proposed solution to observe the trends of stress and displacement components. To be representative, we select the values of $x_0/h = 10^{p_1}$, where $p_1 = 0, 1, 2, 3, 4$. Owing to maximum modulus theorem of complex variable, only the stress and displacement components along both boundaries (the ground surface and tunnel periphery) need to be considered. After substitution and computation, the results are shown in Figs. 5 and 6, respectively. Due to axisymmetry, only the right half geomaterial and corresponding stress and displacement components are illustrated.

Figs. 5 and 6 indicate that when the value of x_0/h gets larger, all the stress and displacement components trend to certain curves. The results strongly suggest convergence of the solution. We should also notice that as the value of x_0/h gets larger, the Gibbs phenomena are first reduced, and are then magnified, indicating that there is an optimum value of x_0/h . The reason is that when x_0/h is very large, the angle of the displacement constraint arc θ_0 in the mapping plane would be very small correspondingly, and the numerical computation would be erratic, as can be seen in Eq. (4.3). Though conceptually a larger value of x_0/h is more mechanically reasonable, the numerical computation accuracy should also be considered for tradeoff. When $x_0/h = 10^2$, all the stress and displacement along the ground surface or tunnel periphery are convergent enough, and the numerical results are also satisfactory. Therefore, the value of $x_0/h = 10^2$ is recommended for actual computation.

6.3 Verification with existing solution

The solution convergence does not necessarily indicate the correctness of the proposed solution. Therefore, a solution comparison should be conducted for verification. We choose the existing modified solution by Lin et al. [Lin et al., 2020] for comparisons. The reasons of choosing this solution are listed below: (1) Both solutions aim at cancelling

the displacement singularity at infinity, but take different measures, which makes the comparisons more valuable than simply verifying the correctness of the proposed solution; to be specific, the proposed solution in this paper takes a mechanical measure of a mixed boundary value problem, while the other solution takes a mathematical measure to simply cancelling the effect of logarithmic item. (2) The assumptions of the proposed solution in this study and the existing modified solution by Lin et al. [Lin et al., 2020] are similar, and the former would degenerate to the latter, when cancelling the displacement constraint along the ground surface. For consistency of accuracy, the programming codes of the modified solution by Lin et al. [Lin et al., 2020] are also rewritten in `fortran`.

Substituting the parameters in Table 1 into both solutions, and $x_0/h = 10^2$ into the proposed solution as well, we obtain the comparisons of stress components along ground surface and tunnel periphery in Fig. 7. Fig. 7 indicates that the stress components for both solutions along tunnel periphery are in agreements. For the ground surface, the stress components between these two solutions slightly deviate. Although the deviation of Figs. 7e and 7f seems obvious and acute, the absolute value of deviation is small, especially comparing to the horizontal stress in Fig. 7d. The reason of the deviation is the remaining effect of the Gibbs phenomena, which *can not be fully eliminated* after reduction, as mentioned at the end of Section 6.1. Fig. 7 indicates that the stress components computed via the proposed solution are identical to those computed via the existing modified solution by Lin et al. [Lin et al., 2020]. The identical stress results further indicate that the solution of d_n in Eq. (4.1) is correct.

The same parameter set obtaining stress is again substituted into the proposed solution to obtain the displacement when $x_0/h = 10^2$. Meanwhile, it should be noted that the displacement of the modified solution by Lin et al. [Lin et al., 2020] further depends on the modified depth H , which is the key parameter to cancelling the displacement singularity at infinity. Such modification is only a purely mathematical strategy and lacks a strong mechanical foundation. We choose the value of $H/h = 10^{p_2}$, where $p_2 = 0, 1, 2, 3$ to compare with the displacement of the proposed solution in this study. The comparing results are shown in Fig. 8.

Figs. 8a and 8b indicate that when H/h is larger than 10^1 , the curve trends of displacement components along tunnel periphery of both solutions are almost the same, and the displacement difference between these two solutions along tunnel periphery is almost a changeable constant for different value of H/h . Owing to axisymmetry, the horizontal displacement of angles $\vartheta = \pm 90^\circ$ in Fig. 8a is expected to be zero, which is identical to the result of the proposed solution in this study, while the horizontal displacement of angles $\vartheta = \pm 90^\circ$ for all four curves of the modified solution by Lin et al. [Lin et al., 2020] are nonzero. Moreover, the parameter $x_0/h = 10^2$ is chosen for the proposed solution in this study, because the displacement components are close to the convergent ones, no matter for the horizontal or the vertical one, as shown in last section. Fig. 8b suggests that the absolute value of the vertical displacement along tunnel periphery of the modified solution by Lin et al. [Lin et al., 2020] would always get larger for a larger value of H/h .

Figs. 8c and 8d provide more information about the displacement difference between the proposed solution in this study and the one by Lin et al. [Lin et al., 2020]. Fig. 8c indicates that as the value of H/h gets larger, the horizontal displacement of the modified solution along the ground surface near the tunnel ($x \leq 100\text{m}$) by Lin et al. [Lin et al., 2020] is more approximate to that by the proposed solution, while the far-field horizontal displacements ($x > 100\text{m}$) between these two solutions are more deviated. Fig. 8d indicates that as the value of H/h gets larger, the vertical displacement of the modified solution along the ground surface near the tunnel ($x \leq 100\text{m}$) by Lin et al. [Lin et al., 2020] is more deviated from the one of the proposed solution in this study.

The results in Section 6.3 indicate that the modified solution by Lin et al. [Lin et al., 2020] is not fully convergent, though this solution eliminates the displacement singularity at infinity in both theoretical and computational aspects. In contrast, the proposed solution has a better convergence than the one by Lin et al. [Lin et al., 2020]. The reason of convergence comes from the mechanical assumption that the far-field ground surface is displacement-constrained ($|x| \geq x_0$), and the constraint provides a constraining force to equilibrate the unbalanced resultant applied along tunnel periphery due to shallow tunnel excavation. In other words, the displacement constraint assumption turn the originally unbalanced resultant problem in Refs [Lin et al., 2020, Lu et al., 2019, Zeng et al., 2019, Lu et al., 2016, Verruijt and Strack, 2008, Verruijt, 1997b,a] into a balanced one with mixed boundaries in this study.

For simpler and deeper understanding, the problem and solution in this study is mechanically and conceptually similar to a one-dimensional cantilever beam subjected to a fixed constraint at one end and an axisymmetrically and longitudinally concentrated force at the other end. The difference is that the dimension of the problem and corresponding solution measure in this paper is elevated from one dimension to two dimensions, and the region in the problem also changes from a simply connected one to a doubly connected one, but the conceptual solution measure remains the same. To be more specific, the static equilibrium in Eq. (4.6) and the single-valuedness of displacement in Eq. (4.12) consist of the mechanical foundation to construct the whole solution and determine the unbalanced resultant along tunnel periphery, while the traction boundary condition in Section 4.3 establishes the remaining neccessary mathematical equations to reach the unique solution of d_n in Eq. (4.1).

7 Parametric investigation and discussion

In this section, a parametric investigation is performed regarding the effects of three distinct parameters in the proposed mechanical model on stress and displacement distribution in geomaterial. The parameters of benchmark model are the same to those in Table 1 (including plain strain condition $\kappa = 3 - 4\nu$), except that $k_0 = 1$ for hydrostatic condition. The free surface range is selected as $x_0/h = 10^2$ in the following Sections 7.1 and 7.2 due to convergence analysis in Section 6.2, and will be altered in Section 7.3 for an extending discussion of the convergence analysis in Section 6.2. To conduct non-dimensional parametric investigation, the stress and displacement in geomaterial are normalized by γh (far-field hydrostatic stress at tunnel center depth) and $u_0 = \frac{\gamma h R}{2G}$ (radial displacement along tunnel periphery subjected to far-field hydrostatic stress γh), respectively. To better evaluate the stress distribution, the pair of non-dimensional maximum and minimum principle stresses ($\sigma_{\max}/\gamma h$ and $\sigma_{\min}/\gamma h$) is used, instead of the three stress components in Eq. (5.4).

7.1 Tunnel depth

Tunnel depth would greatly affect stress and displacement distribution in geomaterial in the proposed mechanical model. The non-dimensional tunnel depths are chosen as $h/R = 1.1, 2, 3$. Substituting all the parameters into the proposed mechanical model, the normalized principle stress and displacement distributions are obtained in Figs. 9 and 10, respectively. Owing to axisymmetry of the proposed mechanical model, only the left or right half geomaterial in physical plane xOy is presented. Such a presentation feature will be used in the following analyses.

The principle stress distributions in Fig. 9 suggest that the maximum and minimum principle stresses generally concentrate at the bottom geomaterial ($\vartheta \in [180^\circ, 360^\circ]$) along tunnel periphery and along the whole of tunnel periphery,

respectively, where the local radial coordinate system $\varrho\vartheta$ in Fig. 1b is used. Therefore, the stress at bottom of tunnel periphery may be monitored during tunnel excavation, and maybe necessary engineering measures may be conducted to prevent possible hazards. Specifically, Fig. 9b suggests a severe tensile stress concentration above tunnel roof, when tunnel depth is very small. Thus, a extremely shallow tunnel should be avoided in design.

Figs. 10a, c, and e suggest that geomaterial near tunnel side walls ($\vartheta \in [-45^\circ, 45^\circ] \cup [135^\circ, 225^\circ]$) horizontally deforms away tunnel cavity. When tunnel depth is small the relative horizontal displacement is larger. Figs. 10b, d, and f suggest that geomaterial generally deforms in a upward manner, which is identical to the upward resultant of shallow tunnel excavation, and the upward deformation of geomaterial near tunnel roof ($\vartheta \in [60^\circ, 120^\circ]$) is the most severe. Displacement oscillations are observed along ground surface due to the reduction of Gibbs phenomena. The deformation of tunnel roof should be monitored during excavation.

7.2 Lateral coefficient

The in-situ lateral coefficient k_0 varies in a certain range, and we select $k_0 = 0.8, 1, 1.2$, which typically present vertical-stress-dominating, hydrostatic, and horizontal-stress-dominating in-situ conditions, respectively. With different k_0 and other parameters, the normalized principle stress and displacement distributions are obtained in Figs. 11 and 12, respectively.

Figs. 11a, c, and e suggest an enlarging area of maximum principle concentration at the bottom of tunnel periphery for an increasing lateral coefficient, and the magnitude of normalized maximum principle stress remains almost the same. Figs. 11b, d, and f, however, suggest a reverse distribution feature of minimum principle stress, when lateral coefficient increases from 0.8 to 1.2. The reason is that $k_0 = 0.8$ and $k_0 = 1.2$ denote the typical in-situ stress conditions of vertical domination and horizontal domination, and tensile areas should be near both tunnel walls and roof-bottom regions, respectively, which is identical to the results in Figs. 11b and f. Stress monitoring at side walls and roof-bottom regions is recommended for excavation in geomaterials of low and high lateral in-situ coefficients, respectively.

Fig. 12a suggests that when lateral coefficient is small ($k_0 = 0.8$), geomaterial near tunnel walls ($\vartheta \in [0^\circ, 60^\circ] \cup [120^\circ, 180^\circ]$) deforms horizontally away from tunnel cavity, while geomaterial near tunnel bottom ($\vartheta \in [210^\circ, 255^\circ] \cup [285^\circ, 330^\circ]$) deforms horizontally towards tunnel cavity. In contrast, Fig. 12e suggests a completely oppisite deformation pattern when lateral coefficient is large ($k_0 = 1.2$). A similar contrast can also be found in Figs. 12b and f. The whole tunnel deforms upwards when lateral coefficient is small ($k_0 = 0.8$), indicating a vertical-stress-dominating in-situ conditions. Meanwhile, the obvious downward displacement near tunnel bottom in Fig. 12f suggest that the tunnel is horizontally squeezed and deforms to a pseudo-ellipse with vertical major axis, indicating a horizontal-stress-dominating in-situ condition. In other words, the tunnel is vertically tensile for large lateral coefficient, which is identical to the minimum principle stress distribution in Fig. 11f.

7.3 Free surface range

The solution convergence regarding the free surface range x_0/h has been validated in Section 6.2, but only along ground surface and tunnel periphery. In this section, validation enhancement is conducted by choosing $x_0/h = 10^0, 10^1, 10^2$, and further discussion is made. Substituting three values of x_0/h and other neccessary parameters into the proposed mechanical model, the normalized principle stress and displacement distributions are obtained in Figs. 13 and 14.

Fig. 13 shows that the stress distribution in geomaterial remains almost the same for different free surface range x_0/h , which indicates that the free surface range would not greatly affect stress distribution in geomaterial (except for the ground surface). The reason is that the displacement constraint along ground surface is a relatively far-field constraint for the geometry combination of $h/R = 2$ in this numerical case, and would spontaneously not greatly alter the stress distribution near tunnel according to Saint Venant Principle.

Fig. 14 suggests an overall increasing trend of upward displacement in geomaterial for a larger free surface range x_0/h , and a similar overall increasing trend of upward displacement in geomaterial is also reported in the analytical solution conducted by Lu et al. [Lu et al., 2021] that a Gaussian-distributed load acts along ground surface. The corresponding finite element verification [Lu et al., 2021] suggests identical results that a larger geomaterial size would greatly increase the overall vertical displacement, even if the Gaussian distributed load remains the same form. As for this study, the increasing free surface range is similar to the larger geomaterial size of geomaterial in the finite element model in Ref [Lu et al., 2021]. Yet it is impossible to build a finite element model of infinitely large lower-half plane, thus, the verification is performed by comparisons with an existing analytical solution in Section 6, instead of a finite element model.

8 Conclusion

This paper proposes a new mechanical model in complex variable method to confront the displacement singularity caused by the unbalanced resultant of shallow tunnel excavation for reasonable stress and displacement in geomaterial. The far-field ground surface displacement is constrained to produce a corresponding constraining force to equilibrate the unbalanced resultant and the original unbalanced problem turns to a static equilibrium one. The constrained far-field ground surface together with the partially free ground surface above the shallow tunnel and the traction distribution along shallow periphery forms mixed boundary value problem, which is converted into a homogenous Riemann-Hilbert problem by applying the analytic continuation. With extra and implicit boundary conditions of the static equilibrium and the displacement single-valuedness in geomaterial, the homogenous Riemann-Hilbert problem is solved using an approximate and iterative method, and the reasonable stress and displacement in geomaterial are obtained. The Lanczos filtering is used to reduce the Gibbs phenomena caused by abrupt change of boundary condition along the ground surface. Several numerical cases are conducted to show that the newly proposed mechanical model successfully and simultaneously guarantee the the convergence and correctness of stress and displacement in geomaterial and eliminate the displacement singularity at infinity. A parametric investigation is made to further discuss the influence of tunnel depth, lateral coefficient, and free surface range on stress and displacement in geomaterial. The proposed mechanical model might also imply that any unbalanced resultant problem of statics in tunnel engineering is better to be converted into a mixed boundary value problem of static equilibrium to obtain reasonable results for both stress and displacement.

Acknowledgement

This study is financially supported by the Natural Science Foundation of Fujian Province, China (Grant No. 2022J05190), the Scientific Research Foundation of Fujian University of Technology (Grant No. GY-Z20094), the National Natural Science Foundation of China (Grant No. 52178318), and the Education Foundation of Fujian Province (Grant No. JAT210287). The authors would like to thank Professor Changjie Zheng, Ph.D. Yiqun Huang, and Associate Professor Xiaoyi Zhang for their suggestions on this study.

A Coefficient degeneration

The complex potentials within region ω can be obtained by repetitive integrations of Eqs. (4.4a) and (4.5).

$$\varphi(\zeta) = iA_{-1} \ln \zeta + a_0 + \sum_{k=1}^{\infty} a_k \zeta^k + \sum_{k=1}^{\infty} b_k \zeta^{-k} \quad (\text{A.1a})$$

$$\psi(\zeta) = -iB_{-1} \ln \zeta + c_0 + \sum_{k=1}^{\infty} c_k \zeta^k + \sum_{k=1}^{\infty} d_k \zeta^{-k} \quad (\text{A.1b})$$

where a_k , b_k , c_k , and d_k corresponding to the same symbols in Refs Verruijt [1997b], Strack and Verruijt [2002], Lu et al. [2016], and can be expanded as:

$$\begin{cases} a_k = i \frac{A_{k-1}}{k} \\ b_k = i \frac{A_{-k-1}}{-k} \end{cases}, \quad k \geq 1 \quad (\text{A.2a})$$

$$\begin{cases} c_k = \frac{1}{2}(iA_{k-2} - iA_k) - i \frac{B_{-k-1}}{k} \\ d_k = \frac{1}{2}(iA_{-k-2} - iA_{-k}) - i \frac{B_{k-1}}{-k} \end{cases}, \quad k \geq 1 \quad (\text{A.2b})$$

and a_0 and c_0 denotes undetermined complex constants due to integration. If we replace the unbalanced resultant along tunnel periphery with a zero resultant traction (similar to the case in Refs Verruijt [1997b]), the unbalanced resultant vanishes, and $A_{-1} = 0$ and $B_{-1} = 0$ should be correspondingly satisfied to eliminate the possible multi-valuedness of the complex potentials in Eq. (A.1). If we further cancel the displacement constraint along the surface near infinity, $A_k = B_k (k \neq -1)$ in Eq. (4.4) is guaranteed and henceforth.

It can be easily verified that with the notations in Eq. (A.2), the equilibriums in Eqs. (21) and (22) in Ref Verruijt [1997b] would be guaranteed. As for $k = 0$, we have

$$c_0 + \bar{a}_0 = \frac{i}{2}(A_{-2} - A_0) \quad (\text{A.3})$$

Since both a_0 and c_0 are integration constants, Eq. (A.3) indicates that $(A_{-2} - A_0)$ should be a constant as well. Since A_0 and A_{-2} are both real due to symmetry, Eq. (A.3) also indicates that $c_0 + \bar{a}_0$ should be a pure imaginary constant. Such a property will be used later on. Subsequently, the coefficients in Eq. (4.14b) can be correspondingly rewritten as

$$e^{-ik\theta} : (r^{-k} - r^k)i \frac{A_{-k-1}}{-k} + (r^{k+2} - r^{-k})i \frac{A_{-k-2}}{-k-1} + (1 - r^2)r^k(iA_k - A_{k-1}), \quad k \geq 1 \quad (\text{A.4a})$$

$$e^{ik\theta} : (r^k - r^{-k})i \frac{A_{k-1}}{k} + (r^{-k+2} - r^k)i \frac{A_{k-2}}{k-1} + (1 - r^2)r^{-k}(iA_{-k} - A_{-k-1}), \quad k \geq 2 \quad (\text{A.4b})$$

$$-r^{-1}e^{i\theta} : i(1 - r^2)(A_0 + A_{-2}) + r^2C \quad (\text{A.4c})$$

$$\text{Constant} : i(1 - r^2)(A_0 + A_{-2}) + C \quad (\text{A.4d})$$

where

$$C = \frac{i}{2}(A_{-2} - A_0) + iC_a = (c_0 + \bar{a}_0) + iC_a$$

should be a pure imaginary constant due to Eq. (A.3). All the coefficients in Eq. (A.4) are multiplied by a constant $\frac{i}{2}$ for simplicity. It can be verified that the coefficients in Eq. (A.4) are respectively identical to the those in Eqs. (29), (28), (31), and (32) in Ref Verruijt [1997b].

B Coefficient expansion in Eq. (4.15b)

The following expansions are necessary:

$$\frac{1}{1 - re^{i\theta}} = \sum_{k=0}^{\infty} r^k e^{ik\theta} \quad (\text{B.1a})$$

$$\ln(1 - re^{i\theta}) = - \sum_{k=1}^{\infty} \frac{r^k}{k} e^{ik\theta} \quad (\text{B.1b})$$

$$\frac{1}{e^{i\theta} - r} = \sum_{k=1}^{\infty} r^{k-1} e^{-ik\theta} \quad (\text{B.2a})$$

$$\frac{1}{(e^{i\theta} - r)^2} = \sum_{k=1}^{\infty} (k-1)r^{k-2} e^{-ik\theta} \quad (\text{B.2b})$$

$$\ln(1 - re^{-i\theta}) = - \sum_{k=1}^{\infty} \frac{r^k}{k} e^{-ik\theta} \quad (\text{B.2c})$$

$$\frac{1}{(1 - re^{i\theta})(e^{i\theta} - r)^2} = \frac{K_1}{1 - re^{i\theta}} + \frac{K_2 e^{i\theta} + K_3}{(e^{i\theta} - r)^2} \quad (\text{B.3})$$

where

$$\begin{cases} K_1 = \frac{r^2}{(1 - r^2)^2} \\ K_2 = \frac{r}{(1 - r^2)^2} \\ K_3 = \frac{1 - 2r^2}{(1 - r^2)^2} \end{cases}$$

Then with substitution of Eqs. (B.1a) and (B.2b), Eq. (B.3) can be expanded as

$$\frac{1}{(1 - re^{i\theta})(e^{i\theta} - r)^2} = \sum_{k=0}^{\infty} f_k e^{ik\theta} + \sum_{k=1}^{\infty} g_k e^{-ik\theta} \quad (\text{B.3'})$$

where

$$\begin{cases} f_k = K_1 r^k \\ g_k = K_2 \cdot k r^{k-1} + K_3 \cdot (k-1) r^{k-2} \end{cases}$$

The following notation is used:

$$\begin{cases} L_1 = -k_0 \gamma a^2 (1 - r^2)^2 \\ L_2 = -\gamma a^2 \\ L_3 = \gamma a^2 r^2 \\ L_4 = \gamma a R \\ L_5 = -\gamma a r R \\ L_6 = \gamma R^2 \end{cases} \quad (\text{B.4})$$

With Eqs. (B.1), (B.2), and (B.3'), E_k in Eq. (4.15b) can be expressed as

$$\begin{cases} E_k = L_1 f_{k-2} + L_2 r^k - L_6 \frac{r^k}{k} + L_6 \frac{r^k}{k-1}, & k \geq 2 \\ E_1 = L_1 g_1 + L_2 r - L_6 r \\ E_0 = L_1 g_2 + L_2 - L_4 r + L_5 - L_6 r^2 \\ E_{-k} = L_1 g_{k+2} + L_3 (k-1) r^{k-2} - L_3 k r^k + L_4 r^{k-1} - L_4 r^{k+1} + L_6 \frac{r^k}{k} - L_6 \frac{r^{k+2}}{k+1}, & k \geq 1 \end{cases} \quad (\text{B.5})$$

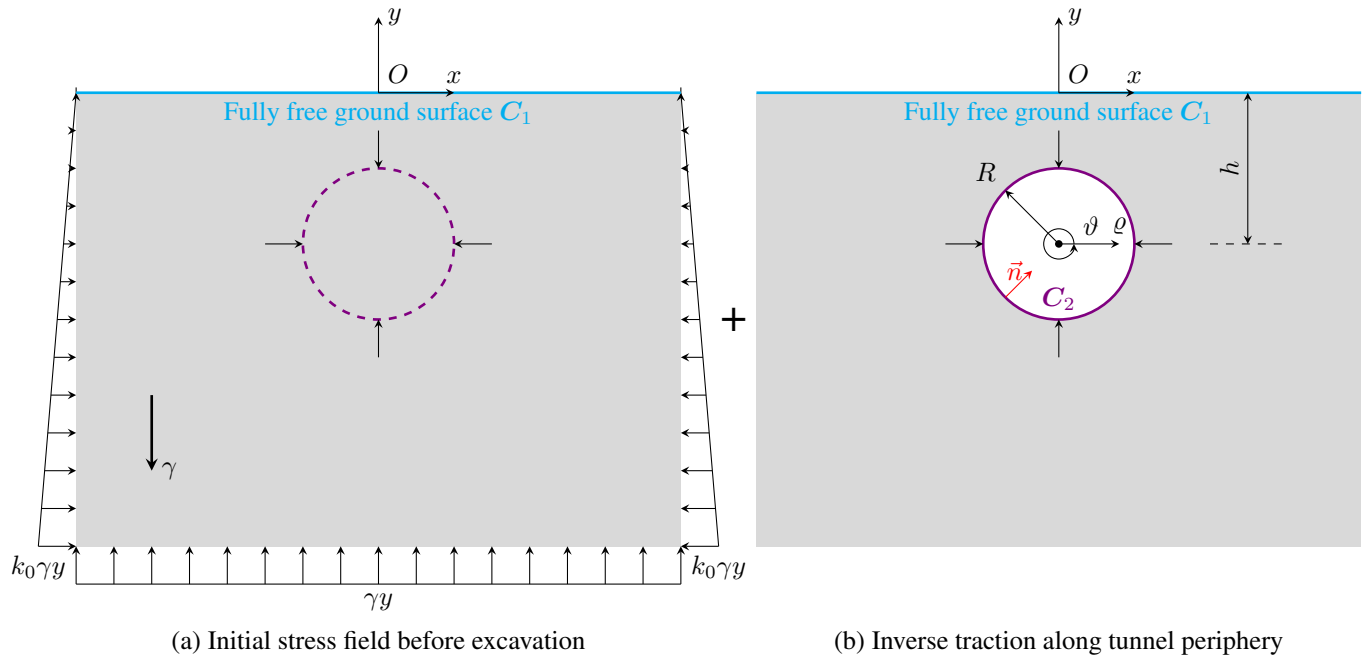


Figure 1: Initial stress field and inverse traction for shallow tunnel excavation

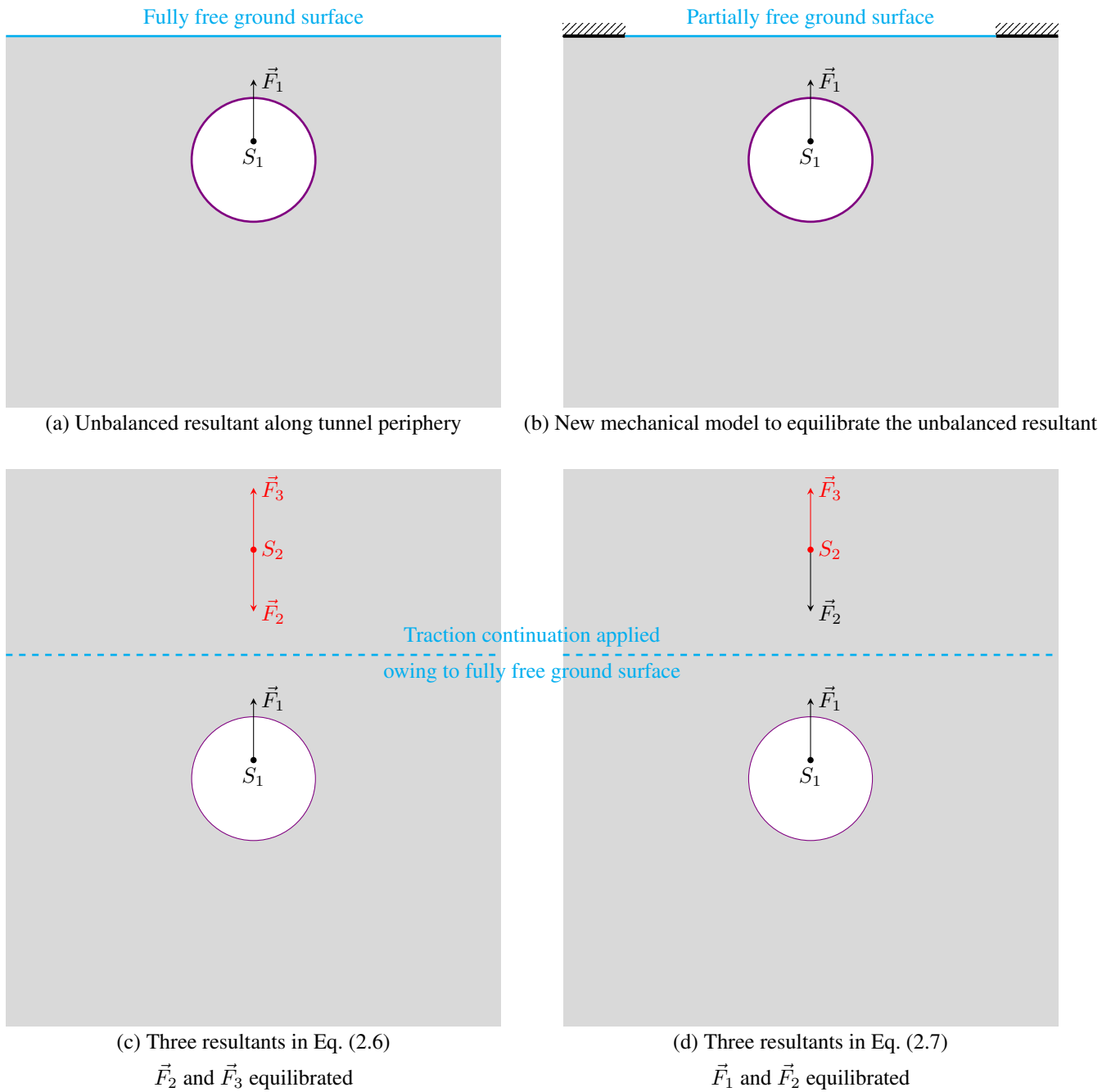


Figure 2: Unbalanced resultants and singularities in geomaterial and sketch of new mechanical model

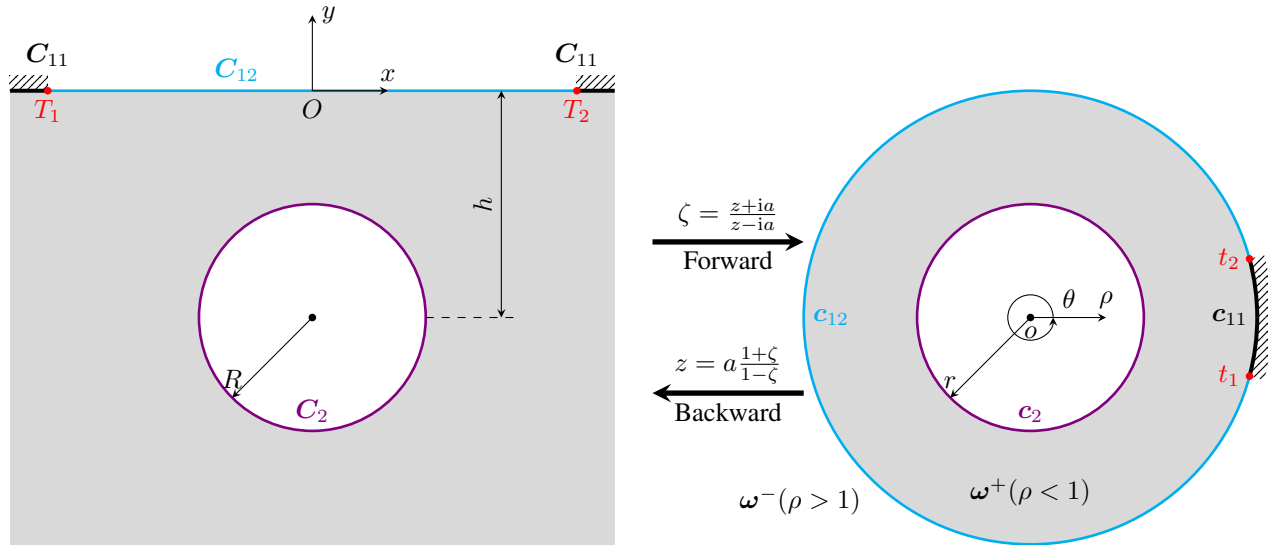
(a) Lower half plane containing a shallow tunnel Ω (b) Unit annulus ω

Figure 3: Schematic diagram of mixed boundary conditions and bidirectional conformal mappings of lower half plane containing a shallow tunnel Ω and unit annulus ω

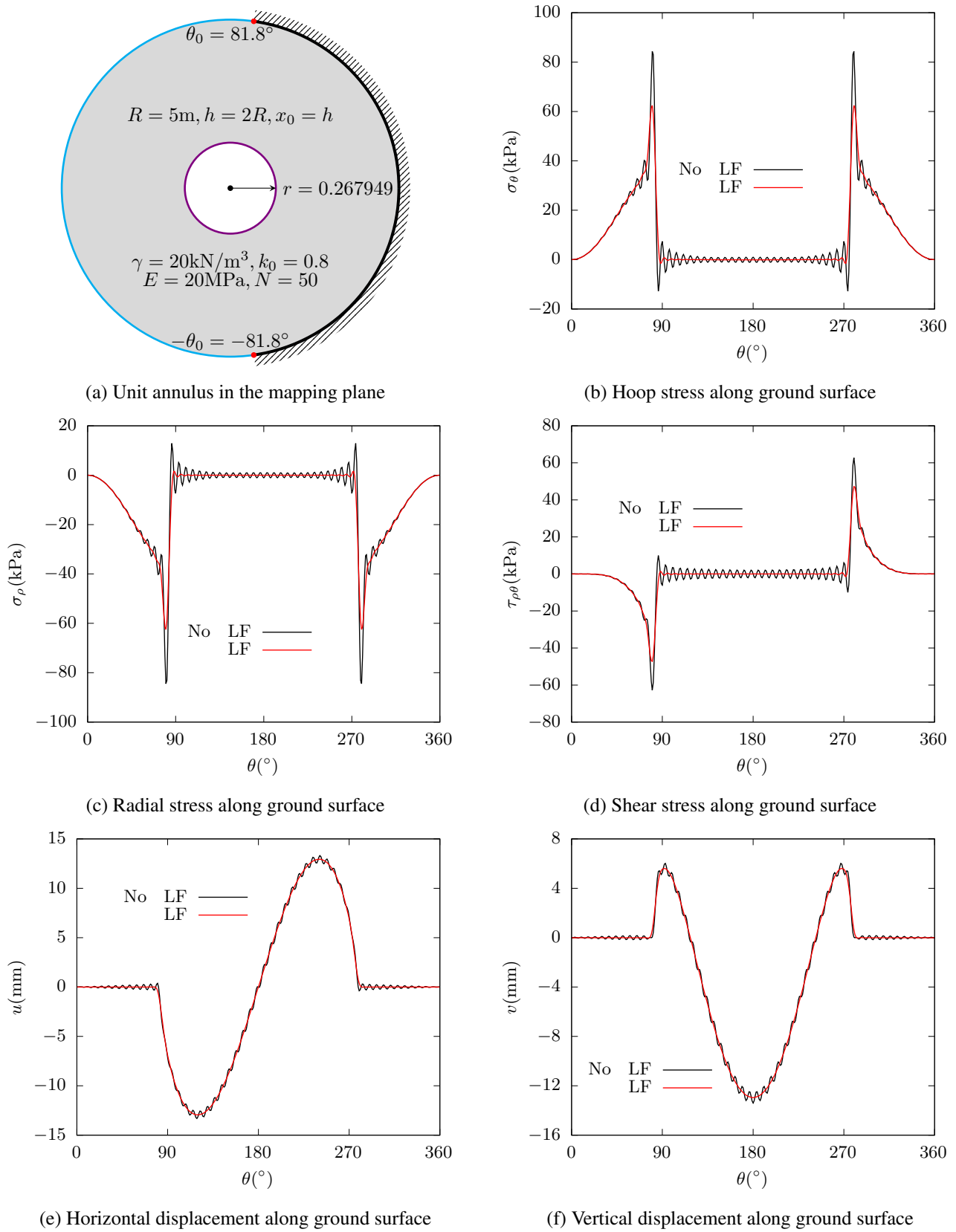


Figure 4: The Lanczos filtering (LF) for stress and displacement components along ground surface in the mapping plane

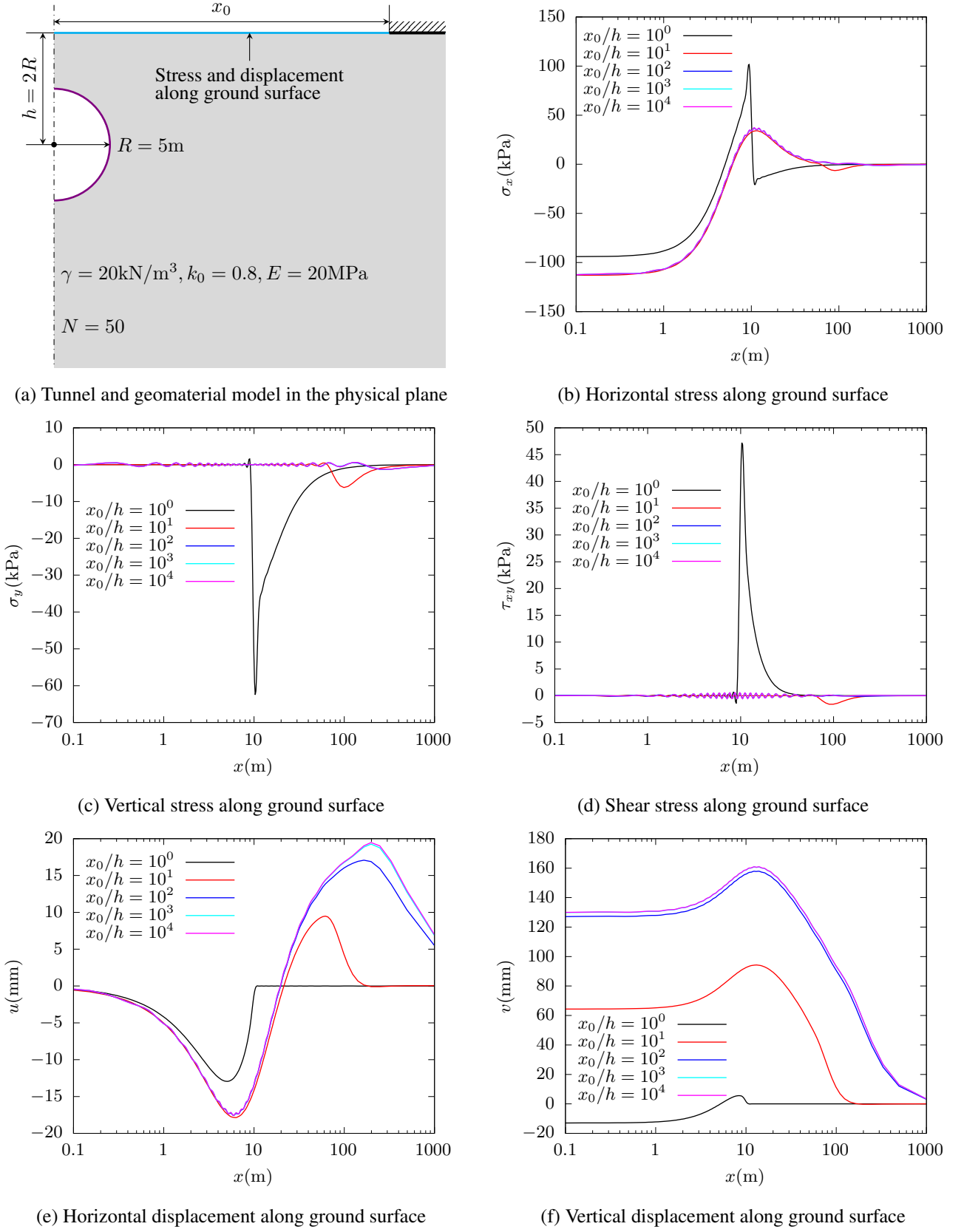


Figure 5: Convergence of stress and displacement components along ground surface

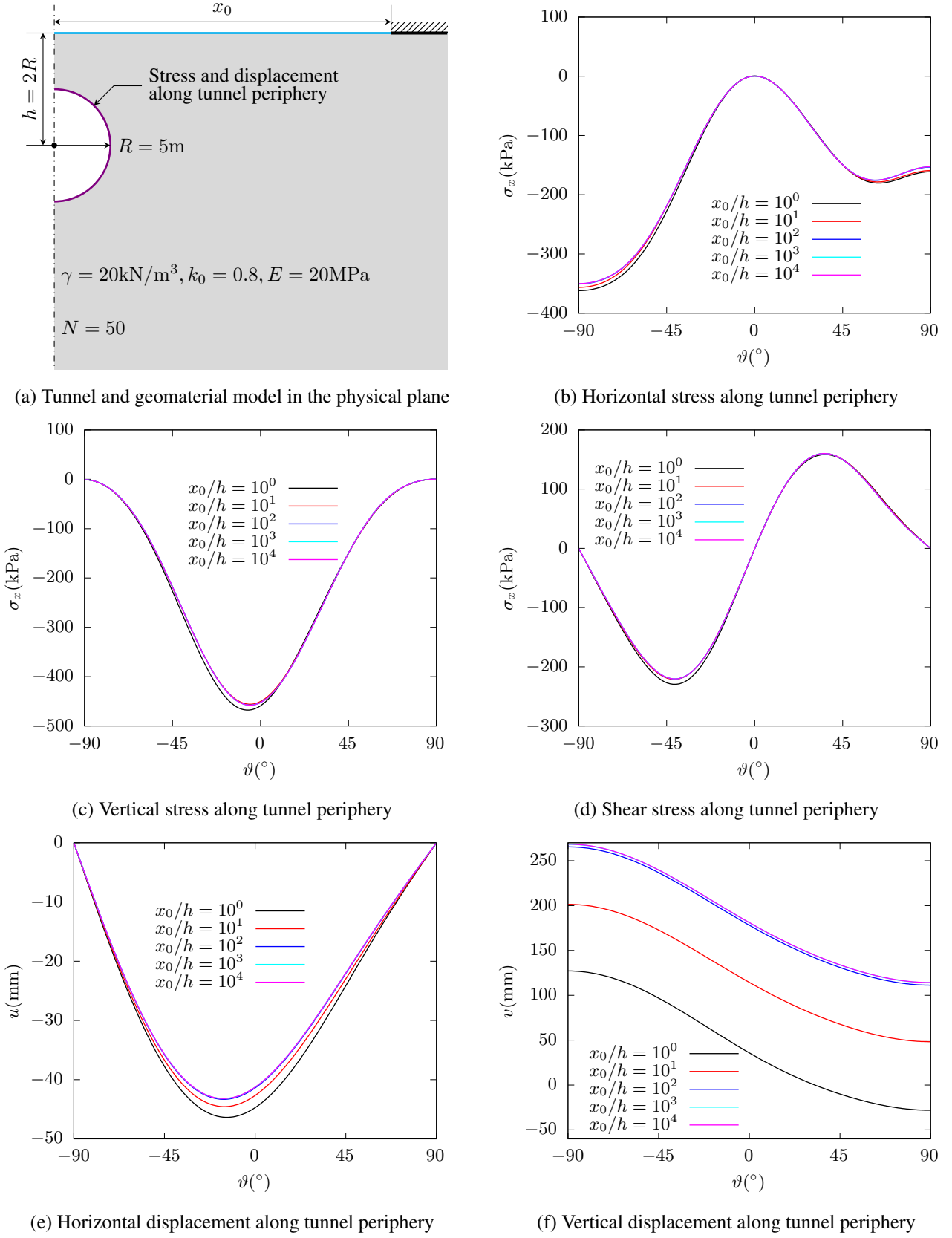


Figure 6: Convergence of stress and displacement along tunnel periphery

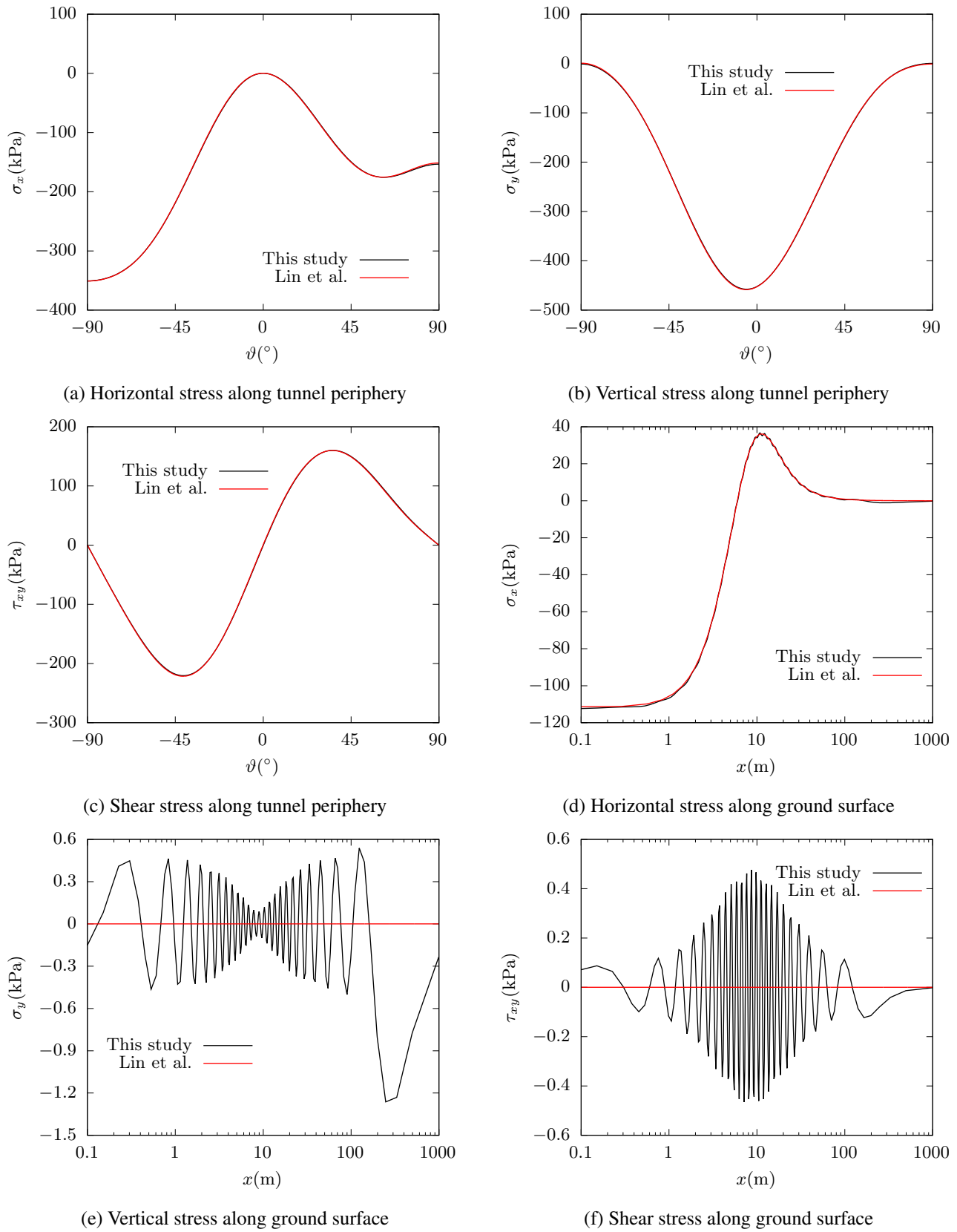


Figure 7: Stress comparisons between present study and Lin et al. [Lin et al., 2020]

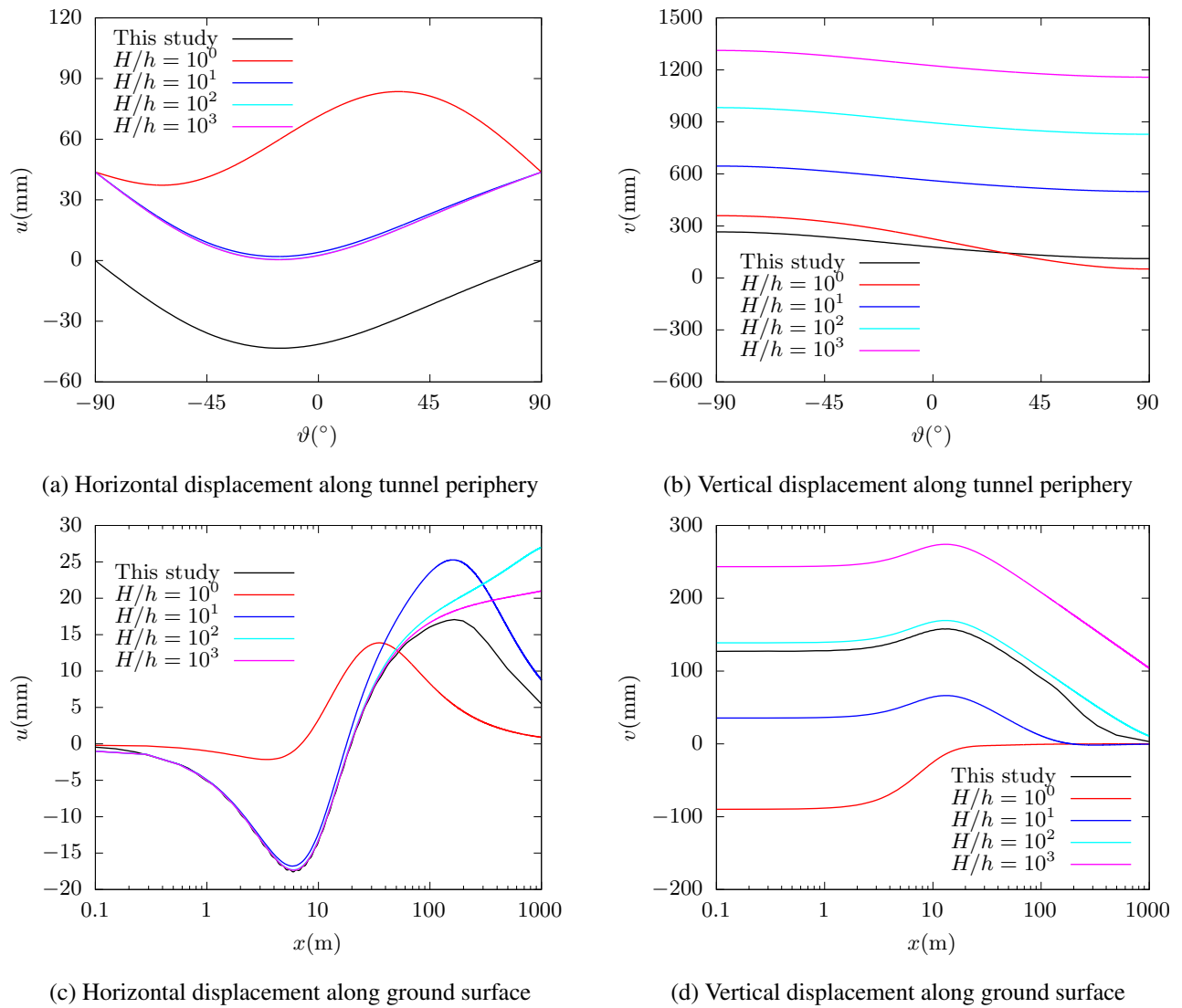


Figure 8: Displacement comparisons between present study and Lin et al. [Lin et al., 2020]

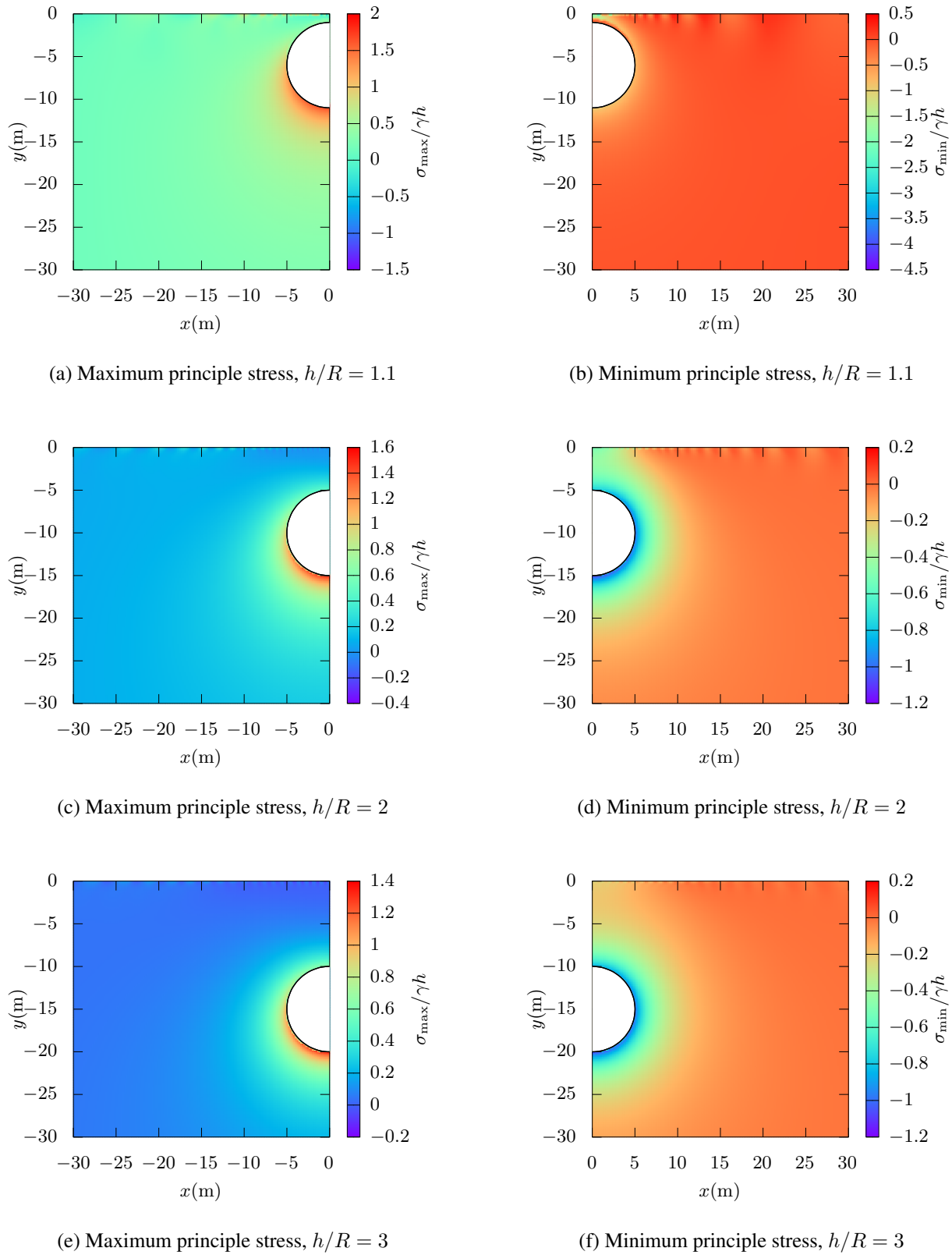


Figure 9: Normalized principle stress distribution against tunnel depth

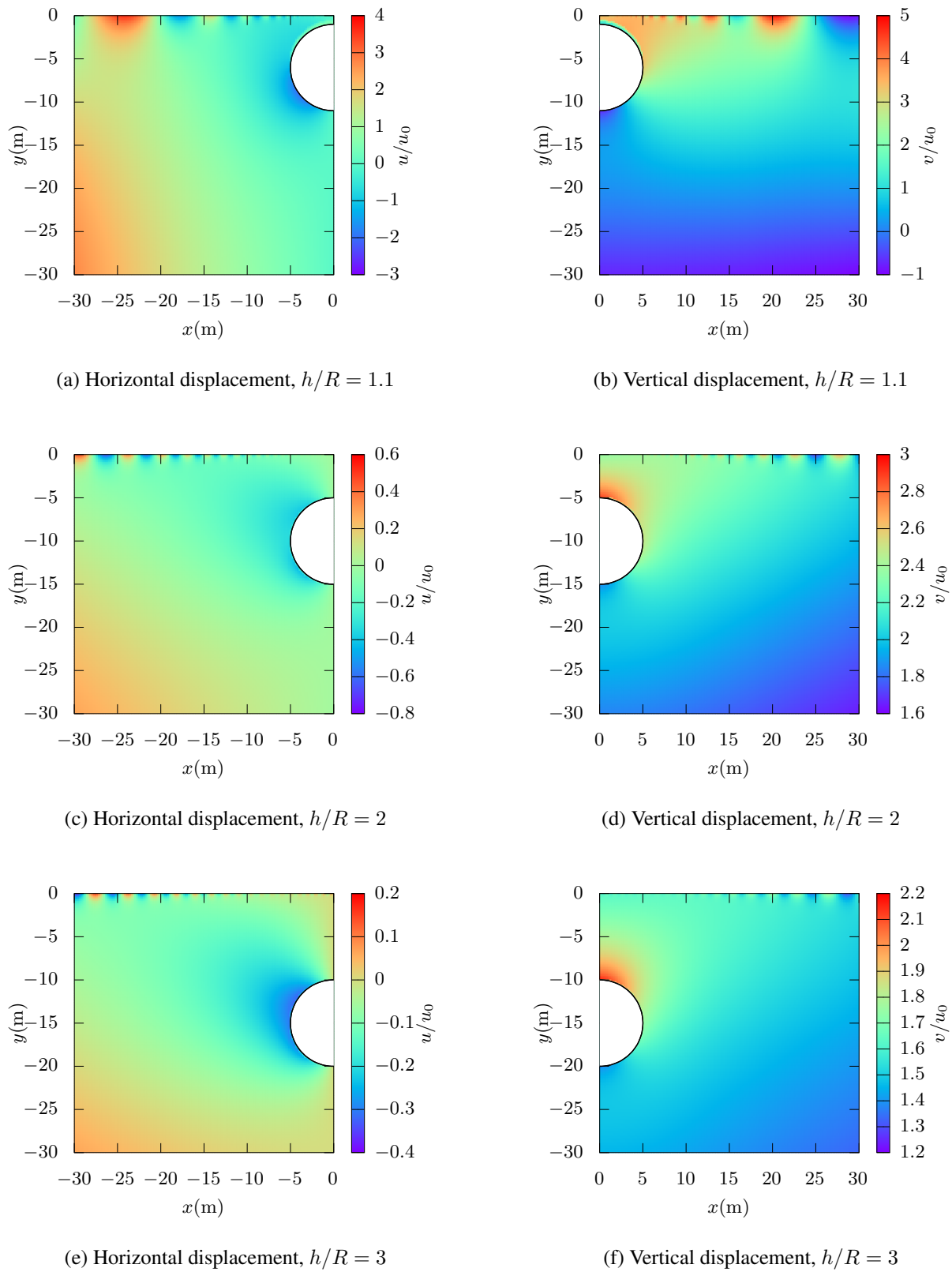


Figure 10: Normalized displacement distribution against tunnel depth

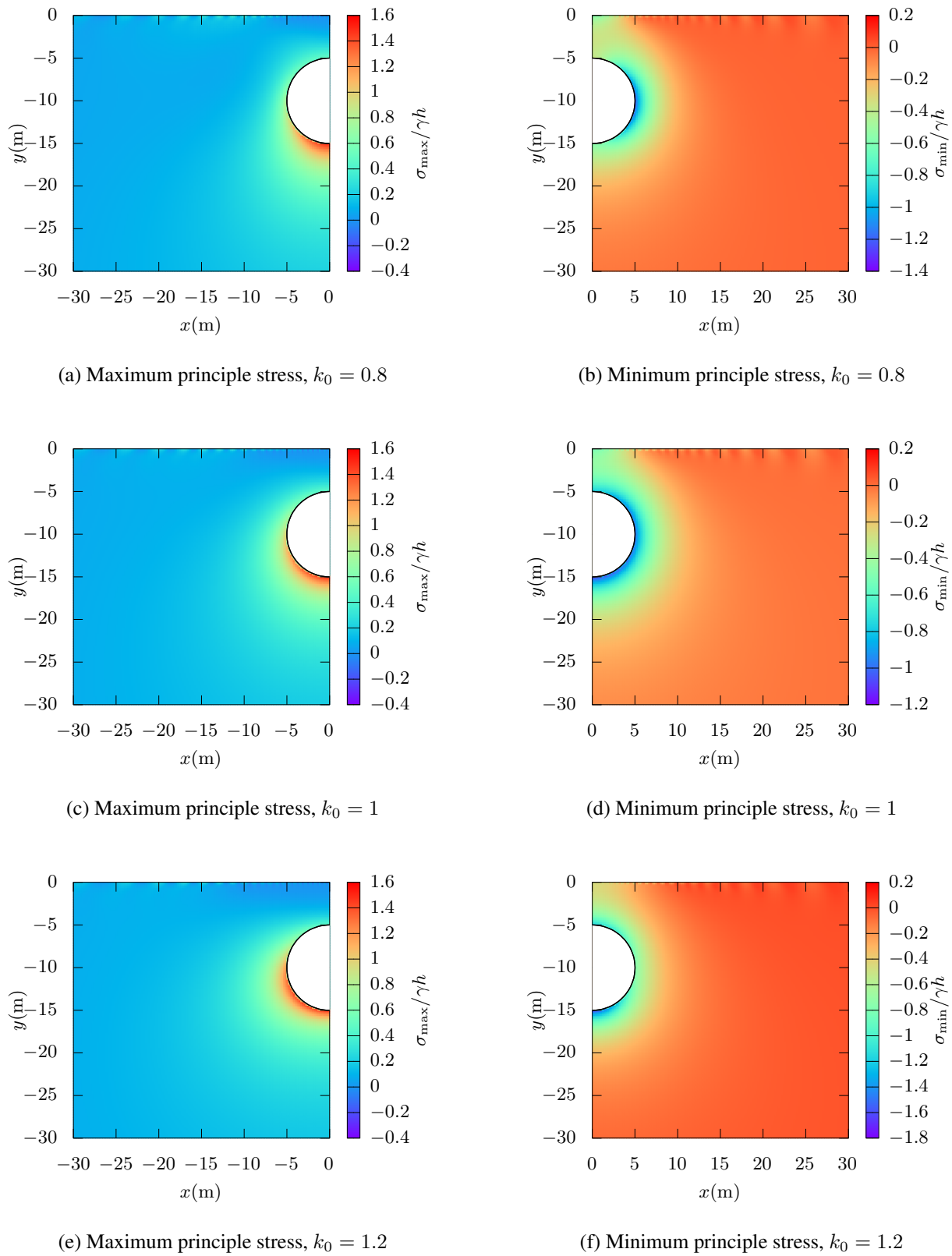


Figure 11: Normalized principle stress distribution against lateral coefficient

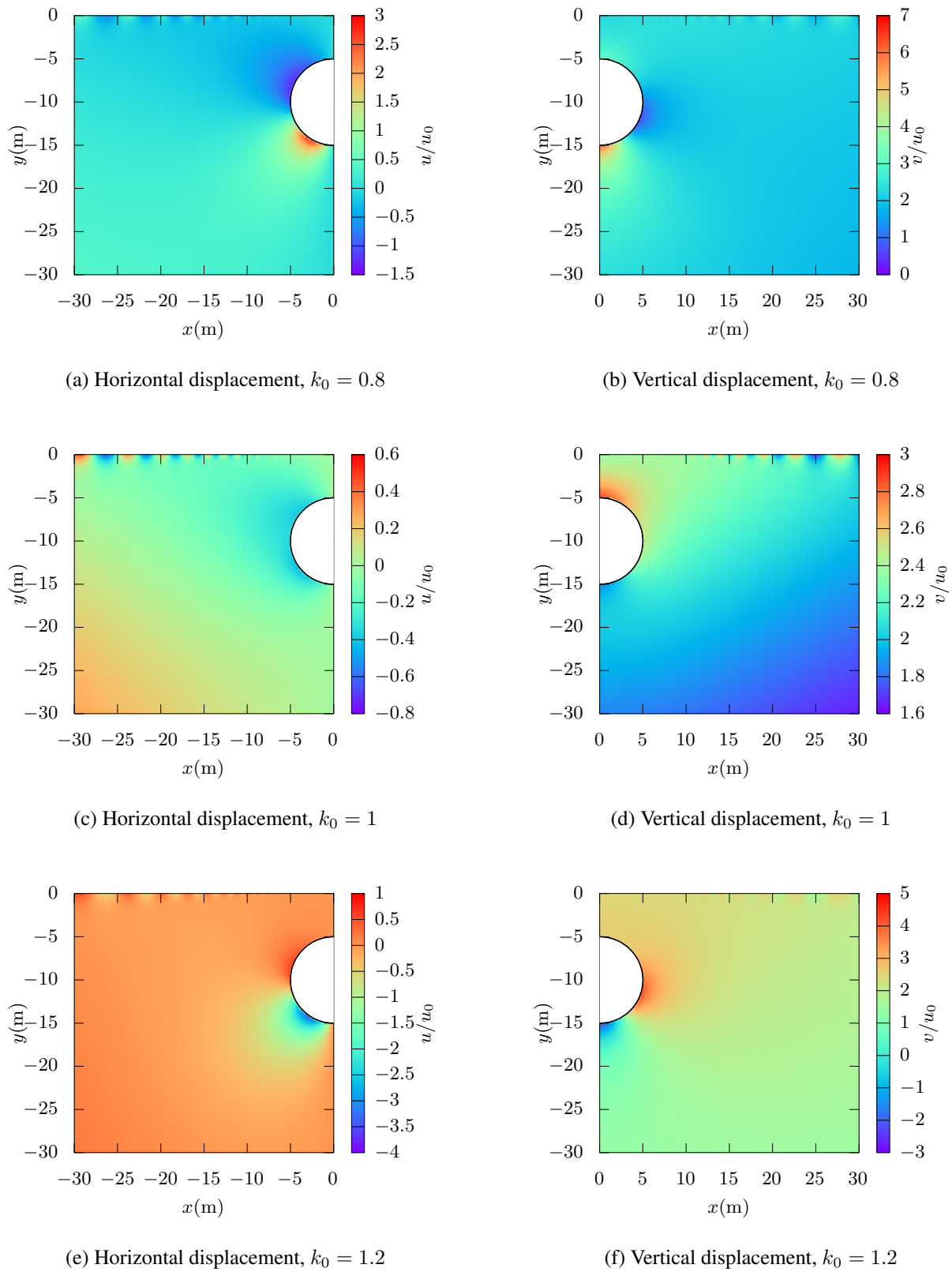


Figure 12: Normalized displacement distribution against lateral coefficient

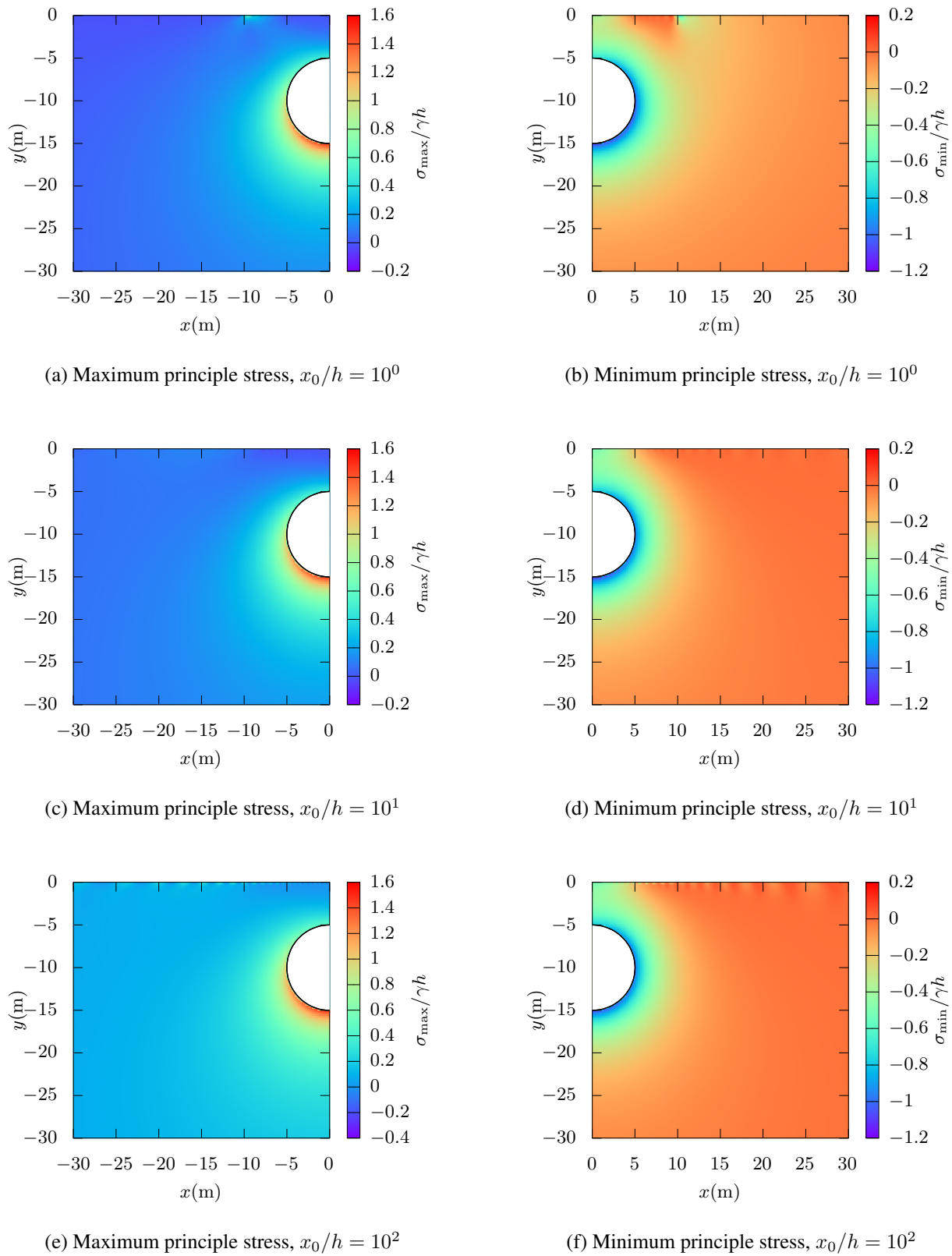


Figure 13: Normalized principle stress distribution against free surface range

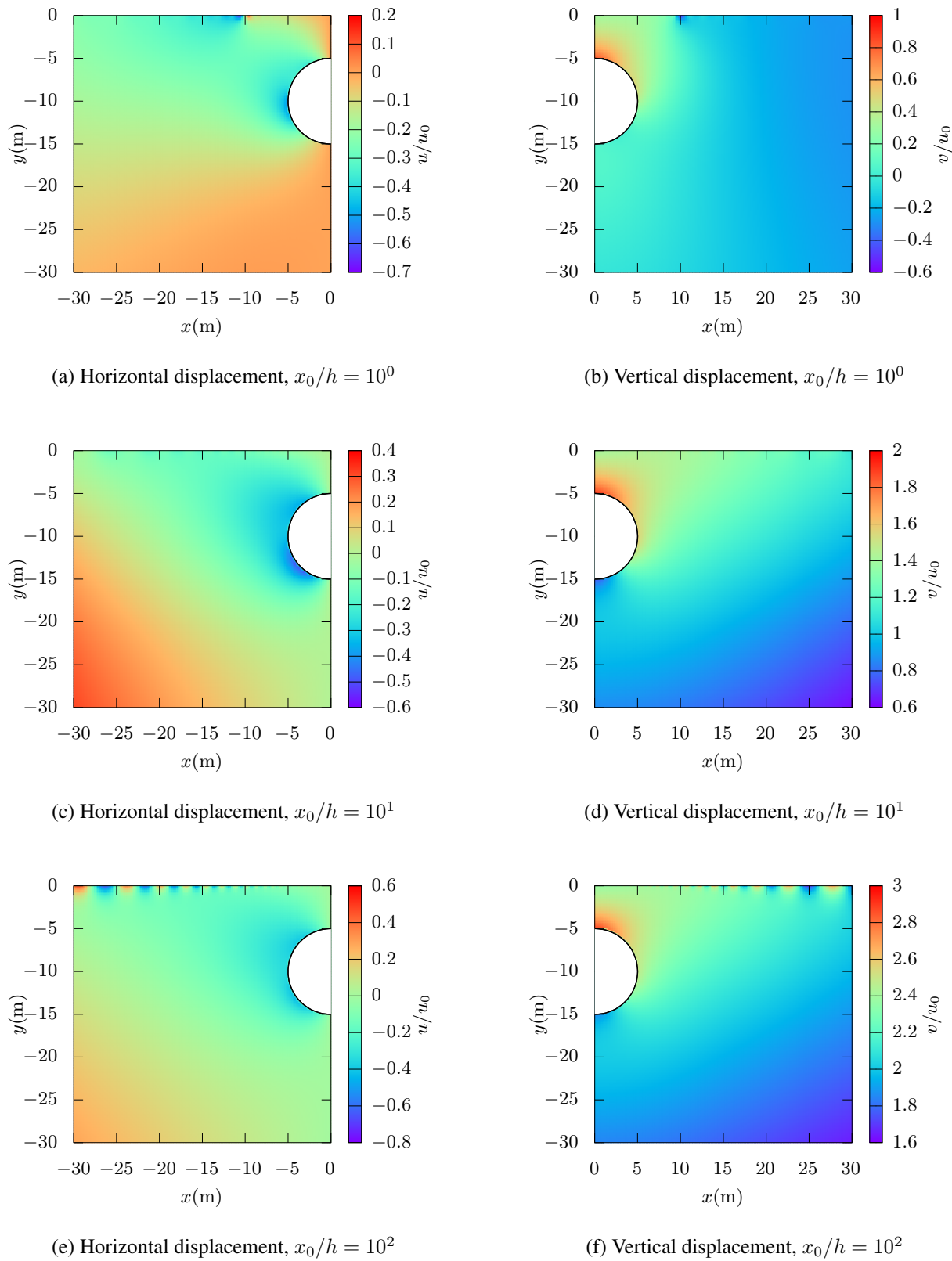


Figure 14: Normalized displacement distribution against free surface range

References

D. P. Chawde and T. K. Bhandakkar. Mixed boundary value problems in power-law functionally graded circular annulus. *International Journal of Pressure Vessels and Piping*, 192:104402, 2021.

Qian Fang, Haoran Song, and Dingli Zhang. Complex variable analysis for stress distribution of an underwater tunnel in an elastic half plane. *International Journal for Numerical and Analytical Methods in Geomechanics*, 39(16):1821–1835, 2015.

A. Flamant. Sur la répartition des pressions dans un solide rectangulaire chargé transversalement. *Comptes Rendus de l'Académie des Sciences Paris*, 114:1465–1468, 1892.

Xiang Gao, Huaning Wang, and Mingjing Jiang. Analytical solutions for the displacement and stress of lined circular tunnel subjected to surcharge loadings in semi-infinite ground. *Applied Mathematical Modelling*, 89:771–791, 2021.

Fanchao Kong, Dechun Lu, Xiuli Du, and Chenpeng Shen. Elastic analytical solution of shallow tunnel owing to twin tunnelling based on a unified displacement function. *Applied Mathematical Modelling*, 68:422–442, 2019.

Fanchao Kong, Dechun Lu, Xiuli Du, Xiaoqiang Li, and Cancan Su. Analytical solution of stress and displacement for a circular underwater shallow tunnel based on a unified stress function. *Ocean Engineering*, 219:108352, 2021.

C. Lanczos. *Applied analysis*. Prentice-Hall, Englewood Cliffs, 1956.

Luobin Lin, Fuquan Chen, and Dayong Li. Modified complex variable method for displacement induced by surcharge loads and shallow tunnel excavation. *Journal of Engineering Mathematics*, 123:1–18, 2020.

Aizhong Lu, Xiangtai Zeng, and Zhen Xu. Solution for a circular cavity in an elastic half plane under gravity and arbitrary lateral stress. *International Journal of Rock Mechanics and Mining Sciences*, 89:34–42, 2016.

Aizhong Lu, Hui Cai, and Shaojie Wang. A new analytical approach for a shallow circular hydraulic tunnel. *Meccanica*, 54(1-2):223–238, 2019.

Aizhong Lu, Yijie Liu, and Hui Cai. A reasonable solution to the elastic problem of half-plane. *Meccanica*, 56(9):2169–2182, 2021.

N. I. Muskhelishvili. *Some basic problems of the mathematical theory of elasticity*. Cambridge University Press, Cambridge, 4th edition, 1966.

G. Singh and T. K. Bhandakkar. Simplified approach to solution of mixed boundary value problems on homogeneous circular domain in elasticity. *Journal of Applied Mechanics*, 86(2):021007, 2019.

O. E. Strack. *Analytic solutions of elastic tunneling problems*. PhD thesis, Delft University of Technology, Amsterdam, 2002.

O. E. Strack and A. Verruijt. A complex variable solution for a deforming buoyant tunnel in a heavy elastic half-plane. *International Journal for Numerical and Analytical Methods in Geomechanics*, 26(12):1235–1252, 2002.

S. P. Timoshenko and J. N. Goodier. *Theory of Elasticity*. McGraw-Hill, New York, 1951.

A. Verruijt. A complex variable solution for a deforming circular tunnel in an elastic half-plane. *International Journal for Numerical and Analytical Methods in Geomechanics*, 21(2):77–89, 1997a.

A. Verruijt. Deformations of an elastic plane with a circular cavity. *International Journal of Solids and Structures*, 35 (21):2795–2804, 1997b.

A. Verruijt and O. E. Strack. Buoyancy of tunnels in soft soils. *Géotechnique*, 58(6):513–515, 2008.

Huaning Wang, Fei Song, and Fang Liu. Modified flamant’s solution for foundation deformation. *Mechanics in Engineering*, 39(3):274–279, 2017.

Huaning Wang, X. P. Chen, Mingjing Jiang, Fei Song, and L. Wu. The analytical predictions on displacement and stress around shallow tunnels subjected to surcharge loadings. *Tunnelling and Underground Space Technology*, 71: 403–427, 2018a.

Huaning Wang, L. Wu, Mingjing Jiang, and Fei Song. Analytical stress and displacement due to twin tunneling in an elastic semi-infinite ground subjected to surcharge loads. *International Journal for Numerical and Analytical Methods in Geomechanics*, 42(6):809–828, 2018b.

Guangshang Zeng, Huaning Wang, and Mingjing Jiang. Analytical solutions of noncircular tunnels in viscoelastic semi-infinite ground subjected to surcharge loadings. *Applied Mathematical Modelling*, 102:492–510, 2022.

Guisen Zeng, Hui Cai, and Aizhong Lu. An analytical solution for an arbitrary cavity in an elastic half-plane. *Rock Mechanics and Rock Engineering*, 52:4509–4526, 2019.

Zhiguo Zhang, Maosong Huang, Xiaoguang Xi, and Xuan Yang. Complex variable solutions for soil and liner deformation due to tunneling in clays. *International Journal of Geomechanics*, 18(7):04018074, 2018.

Zhiguo Zhang, Maosong Huang, Yutao Pan, Kangming Jiang, Zhenbo Li, Shaokun Ma, and Yangbin Zhang. Analytical prediction of time-dependent behavior for tunneling-induced ground movements and stresses subjected to surcharge loading based on rheological mechanics. *Computers and Geotechnics*, 129:103858, 2021.